

สเปกโทรสโกปีการดูดกลืนรังสีเอกซ์ของโครงสร้างไว้ระเบียนสองระบบ:
โครงสร้างไฮเดรชันของ Ca^{2+} และโครงสร้างซิงค์ออกซิได์ในไตรด์

นายธีรวัฒน์ ม่อนหน่อ

วิทยานิพนธ์นี้เป็นส่วนหนึ่งของการศึกษาตามหลักสูตรปริญญาวิทยาศาสตรมหาบัณฑิต
สาขาวิชาฟิสิกส์
มหาวิทยาลัยเทคโนโลยีสุรนารี
ปีการศึกษา 2552

**X-RAY ABSORPTION SPECTROSCOPY OF TWO
DISORDERED SYSTEMS: Ca²⁺ HYDRATION
STRUCTURE AND ZINC OXYNITRIDE STRUCTURE**

Teerawat Monnor

**A Thesis Submitted in Partial Fulfillment of the Requirements for the
Degree of Master of Science in Physics
Suranaree University of Technology
Academic Year 2009**

**X-RAY ABSORPTION SPECTROSCOPY OF TWO
DISORDER SYSTEMS: Ca²⁺ HYDRATION STRUCTURE AND
ZINC OXYNITRIDE STRUCTURE**

Suranaree University of Technology has approved this thesis submitted in
partial fulfillment of the requirements for a Master's degree

Thesis Examining Committee

(Asst. Prof. Dr. Chinorat Kobdaj)

Chairperson

(Dr. Saroj Rujirawat)

Member (Thesis Advisor)

(Prof. Dr. Sukit Limpijumnong)

Member

(Assoc. Prof. Dr. Anan Tongraar)

Member

(Asst. Prof. Dr. Rattikorn Yimnirun)

Member

(Prof. Dr. Sukit Limpijumnong)

Vice Rector of Academic Affairs

(Assoc. Prof. Dr. Prapun Manyum)

Dean of Institute of Science

ธีรวัฒน์ ม่อนหน่อ : สเปกโทรสโกปีการดูดกลืนรังสีเอกซ์ของโครงสร้างไร้ระเบียบสองระบบ: โครงสร้างไฮเดรชันของ Ca^{2+} และโครงสร้างซิงค์ออกไซด์ในไตรด์ (X-RAY ABSORPTION SPECTROSCOPY OF TWO DISORDERED SYSTEMS: Ca^{2+} HYDRATION STRUCTURE AND ZINC OXYNITRIDE STRUCTURE)
อาจารย์ที่ปรึกษา : อ. ดร. สาโรช รุจิรวรรณ, 70 หน้า.

วัตถุที่มีโครงสร้างไร้ระเบียบ ซึ่งปราศจากสมบัตินี้การมีโครงสร้างแบบเป็นคาบนั้น ยากที่จะถูกศึกษาด้วยวิธีมาตรฐาน เช่น การเลี้ยวเบนรังสีเอกซ์ หรือ กล้องจุลทรรศน์อิเล็กตรอนกำลังแยกแยะสูง ในการศึกษาครั้งนี้จึงได้เสนอวิธีการสเปกโทรสโกปีการดูดกลืนรังสีเอกซ์เป็นทางเลือกหนึ่ง เพื่อใช้ศึกษาโครงสร้างระดับอะตอมของระบบไร้ระเบียบ โดยสองระบบที่ถูกเลือกศึกษา คือ โครงสร้างไฮเดรชันของ Ca^{2+} และโครงสร้างฟิล์มบางของซิงค์ออกไซด์ในไตรด์ โดยได้ใช้วิธีการดูดกลืนรังสีเอกซ์ในช่วง XANES และ EXAFS ในการศึกษาครั้งนี้ โดยแบบจำลองโครงสร้างไฮเดรชันของ Ca^{2+} ที่เลือกใช้ได้จากวิธี QM/MM ซึ่งคำนวณโดย รศ. ดร. อนันต์ ทองระอา และฟิล์มบางของสารซิงค์ออกไซด์ในไตรด์ได้ถูกเตรียมโดยกลุ่มวิจัยของ รศ. ดร. จิติ หนูแก้ว ซึ่งผลการวัดได้ถูกวิเคราะห์ให้ได้มาซึ่งตัวแปรโครงสร้างที่สำคัญ

สำหรับการศึกษาโครงสร้างของน้ำล้อมรอบไอออนแคลเซียมนั้น EXAFS ให้ระยะพันธะ Ca-O เฉลี่ย $2.431 \pm 0.011 \text{ \AA}$ เลขโคออร์ดิเนชัน 6.56 ± 0.316 และ ค่าสัมประสิทธิ์เดอบาย-วอลเลอร์ 0.009 \AA^2 โดยค่าที่ได้สำหรับตัวแปรเหล่านี้มีความสอดคล้องกันเป็นอย่างดีกับตัวแปรที่ได้จาก RDF ของแบบจำลองทางทฤษฎีตาม QM/MM คือ 2.445 \AA , 6.8 และ 0.0096 \AA^2 ตามลำดับ นอกจากนี้สเปกตรัม XANES ที่ได้จากการวัด ยังเข้ากันได้ดีกับสเปกตรัม XANES ที่ได้จากการคำนวณจากแบบจำลอง QM/MM ซึ่งผลการวิเคราะห์ที่ได้สามารถสนับสนุนความถูกต้องของแบบจำลอง QM/MM ได้เป็นอย่างดี

ในการศึกษาโครงสร้างฟิล์มบางซิงค์ออกไซด์ในไตรด์ แบบจำลองได้ถูกสร้างขึ้นจากองค์ประกอบหลักที่รู้จักโดยใช้การวิเคราะห์แบบ linear combination ผลการวิเคราะห์สเปกตรัม XANES แสดงให้เห็นว่าวัสดุตัวอย่างดังกล่าวนี้ ประกอบด้วย ซิงค์ออกไซด์ และ โลหะสังกะสี ที่ปะปนกันเป็นผลึกขนาดนาโนเป็นหลัก

TEERAWAT MONNOR : X-RAY ABSORPTION SPECTROSCOPY OF
TWO DISORDER SYSTEMS: Ca²⁺ HYDRATION STRUCTURE AND
ZINC OXYNITRIDE STRUCTURE. THESIS ADVISOR SAROJ
RUJIRAWAT, Ph.D. 70 PP.

X-RAY ABSORPTION SPECTROSCOPY/HYDRATION STRUCTURE
/DISORDER SYSTEM

Disorder materials with no long-range periodic structure are difficult to be characterized by standard methods, such as x-ray diffraction or high resolution electron microscopy. In this work, x-ray absorption spectroscopy (XAS) was proposed as an alternative way to study the atomic structure of disorder systems. Two selected disorder systems: Ca²⁺_{aq} and zinc oxynitride thin films were studied by x-ray absorption near edge structures (XANES) and extended x-ray absorption fine structure (EXAFS). The candidate structural model for Ca²⁺_{aq} was based on Quantum mechanics/Molecular mechanics (QM/MM) simulation by A. Tongraar. The zinc oxynitride thin films were obtained from J. Nukeaw. The measurement data were analyzed to obtain the important structural parameters to be compared with the calculated spectra.

For the study of Ca²⁺ hydration structure, EXAFS give an average Ca-O bond distance of 2.431 ± 0.011 Å, a coordination number of 6.56 ± 0.316 and a Debye-Waller factor of 0.009 Å². These parameters agreed well with the parameters obtained from RDF of the theoretical QM/MM simulation of 2.445 Å, 6.8 and 0.0096 Å², respectively. The measured XANES spectrum can be fitted very well with that obtained from QM/MM. This result strongly supported the accuracy of QM/MM model.

On the structural investigation of zinc oxynitride thin films, the model compounds were constructed from known reference compounds using a linear combination analysis (LCA). The XANES result suggested that the material mainly contained mixing ZnO nanocrystals and zinc metal nanocrystals.

School of Physics

Academic Year 2009

Student's Signature _____

Advisor's Signature _____

ACKNOWLEDGEMENTS

I would like to acknowledge my advisor Dr. Saroj Rujirawat for his generous helps and advices. Despite his busy schedule, he always pays a lot of attention on his advisees. My master study has been great under his supervision. Dr. Jiraroj T-Thienprasert is the next person who I would like to convey my appreciation to his kind help. In addition, my thesis can not be completed without the contributions from all thesis-examining committees. Therefore, I would like to thank them for all valuable advices.

I would like to acknowledge School of Physics, Suranaree University of Technology for offering me a chance to express my curiosities, and Synchrotron Light Research Institute for benevolent financial support. Furthermore, I would like to acknowledge lecturers and friends in the school for academic and non-academic help.

I also would like to thank my family and all my friends for their precious supports and encouragements.

Teerawat Monnor

CONTENTS

	Page
ABSTRACT IN THAI.....	IV
ABSTRACT IN ENGLISH.....	V
ACKNOWLEDGEMENTS.....	VII
CONTENTS.....	VIII
LIST OF TABLES.....	X
LIST OF FIGURES.....	XI
LIST OF ABBREVIATIONS.....	XVI
CHAPTER	
I INTRODUCTION.....	1
1.1 Background on Ca ²⁺ hydration structure.....	2
1.2 Background on Zinc oxynitride alloys.....	8
1.3 Research objectives.....	10
1.4 Scope and limitation of the study.....	10
II RESEARCH METHODOLOGY.....	12
2.1 X-ray absorption spectroscopy.....	12
2.1.1 X-ray absorption near-edge structure (XANES).....	15
2.1.2 Extended x-ray absorption fine structure (EXAFS).....	16
2.2 X-ray absorption spectroscopy experimental set up.....	19
2.3 X-ray absorption spectrum calculation.....	22
2.3.1 FEFF code overview.....	22
2.3.2 XAS calculation.....	25

CONTENTS (Continued)

	Page
2.4 X-ray absorption spectroscopy spectra analysis.....	29
2.5 Ca ²⁺ hydration simulation by QM/MM modeling.....	36
2.6 Zinc oxynitride alloys.....	40
III STRUCTURAL ANALYSIS OF Ca²⁺ HYDRATION STRUCTURE.....	43
3.1 XAS measurement of Ca ²⁺ _{aq}	43
3.2 Generation theoretical EXAFS spectra.....	45
3.3 EXAFS Analysis.....	48
3.4 XANES Analysis.....	53
IV STRUCTURAL ANALYSIS OF ZINC OXYNITRIDE ALLOYS.....	61
V CONCLUTIONS.....	69
REFERENCES.....	72
APPENDIX.....	77
CURRICULUM VITAE.....	79

LIST OF TABLES

Table	Page
1.1 Results from theoretical predictions for Ca^{2+} hydration structure: R_0 is nearest neighbor distance, σ^2 is Debye-Waller factor, and N is coordination number.....	4
1.2 The main structural parameters of Ca^{2+} hydration structure from various experimental studies.....	7
1.3 Results from experimental studies of zinc oxynitride.....	10
3.1 Results from theoretical simulations for $\text{Ca}^{2+}_{\text{aq}}$ structural parameters: R_0 is nearest neighbor hydration shell distance, N is coordination number and σ^2 is Debye-Waller factor.....	48
3.2 Fitting result for $\text{Ca}^{2+}_{\text{aq}}$ structural parameters of the measured EXAFS.....	50
3.3 Results from the EXAFS fitting for $\text{Ca}^{2+}_{\text{aq}}$ structural parameters compared with the results published in the literature.....	51
3.4 Fitting for $\text{Ca}^{2+}_{\text{aq}}$ structural parameters of the calculated EXAFS spectrum.....	52
4.1 Proportion of ZnO and Zn metal, and R-factor of three unknown samples obtained from linear combination analysis.....	67

LIST OF FIGURES (Continued)

Figure	Page
2.8 XAS experimental set up at the Siam Photon Laboratory, Synchrotron Light Research Institute.....	21
2.9 The excited state (a) x-ray fluorescence and (b) the Auger effect.....	22
2.10 Detail of “feff.inp” input file of ZnO with Zn as center atom for FEFF calculation.....	24
2.11 Detail of atoms.inp input file to generate “feff.inp” for FEFF calculation.....	25
2.12 Schematic illustration of muffin-tin potential in two dimensions (Rehr and Albers, 2000).....	27
2.13 Calculated Zn K-edge XANES of ZnO with different SCF parameters.....	28
2.14 Calculated Zn K-edge XANES of ZnO with different FMS parameters.....	29
2.15 Pre-edge background subtractions for measured $\text{Ca}^{2+}_{\text{aq}}$ K-edge XAS spectrum.....	31
2.16 Post-edge line or normalization line for measured $\text{Ca}^{2+}_{\text{aq}}$ K-edge XAS spectrum.....	31
2.17 Normalized K-edge XAS spectrum for $\text{Ca}^{2+}_{\text{aq}}$	32
2.18 K-edge EXAFS spectrum in k space ($\chi(k)$) for $\text{Ca}^{2+}_{\text{aq}}$	33
2.19 k^2 -weighed K-edge EXAFS spectrum for $\text{Ca}^{2+}_{\text{aq}}$	34
2.20 k^2 -weighed K-edge EXAFS for $\text{Ca}^{2+}_{\text{aq}}$ with Handing window.....	35
2.21 K-edge EXAFS spectrum in real space $\chi(R)$ for $\text{Ca}^{2+}_{\text{aq}}$	35
2.22 Schematic illustration of QM/MM modeling of QM and MM region.....	38
2.23 A snapshot of Ca^{2+} hydration structure by QM/MM simulation.....	39

LIST OF FIGURES (Continued)

Figure	Page
2.24 The trajectories of water molecules with respected to Ca^{2+} (Ca-O distances) from QM/MM calculation within 50 ps. The first hydration shell is clearly seen. Some molecules have entered or left the first shell in this simulation duration.....	39
2.25 Ball-and-stick models for (a) zinc oxide (ZnO) and (b) zinc nitride (Zn_2N_3) and (c) $\text{ZnO}_{0.5}\text{N}_{0.5}$ (d) Zn metal.....	41
3.1 Normalized K-edge XAS spectrum of $\text{Ca}^{2+}_{\text{aq}}$. Shown in the lower and upper insets are [1s3d] and [1s3p] excitation channels.....	44
3.2 k^2 -weighted theoretical EXAFS spectra of $\text{Ca}^{2+}_{\text{aq}}$ from 50 snapshots each separated by 0.5 ps time step. The average spectrum is shown in solid black line.....	45
3.3 Fitting of radial distribution function (datched line) with Gaussian distribution function (solid line).....	47
3.4 Comparison of k^2 -weighted EXAFS spectra of $\text{Ca}^{2+}_{\text{aq}}$: theoretical QM/MM spectrum, measurement spectrum, and fitting.....	49
3.5 Comparison of Fourier transforms of EXAFS spectra of $\text{Ca}^{2+}_{\text{aq}}$: theoretical QM/MM spectrum, measurement spectrum, and fitting.....	49
3.6 Comparison of (a) k-space and (b) real space EXAFS spectra of $\text{Ca}^{2+}_{\text{aq}}$: theoretical QM/MM spectrum (solid line) and its fitting (dashed line).....	52
3.7 Calculated K-edge XANES spectra of $\text{Ca}^{2+}_{\text{aq}}$ hydration structure from model Ca-O structures compared with the measurement spectrum (dashed-line).....	54

LIST OF FIGURES (Continued)

Figure	Page
3.8	Calculated K-edge XANES spectra of $\text{Ca}^{2+}_{\text{aq}}$ hydration structure from 50 QM/MM snapshots with 0.5 ps time step, all shown in gray line. The average spectrum is shown in black line.....57
3.9	K-edge XANES spectra of $\text{Ca}^{2+}_{\text{aq}}$ from four QM/MM snapshots (solid line) compared with experimental data (dashed line). The insets are correspondent Ca^{2+} hydration structure models within the first shell.....58
3.10	Comparison between experimental (dashed) and theoretical QM/MM (hatched) K-edge XANES spectra of $\text{Ca}^{2+}_{\text{aq}}$59
4.1	Zn K-edge XANES normalized spectra of three zinc oxynitride samples.....62
4.2	Comparison of the measured Zn K-edge XANES spectra of zinc oxynitride, and simulated spectrum from ZnO and $\text{ZnO}_{0.5}\text{N}_{0.5}$ alloys.....64
4.3	Comparison of the measured Zn K-edge XANES spectra of zinc oxynitride and simulated spectra from linear combination of ZnO and Zn_3N_2 with various proportions.....65
4.4	Comparison of the measured Zn K-edge XANES spectra of zinc oxynitride and the reference spectra of ZnO and Zn metal.....66
4.5	K-edge XANES of zinc oxynitride samples (a) and their fitting (b).....67
5.1	A diagrammatic procedure for studying of disorder system by XAS.....71

LIST OF ABBREVIATIONS

EXAFS	= Extended x-ray absorption fine structure
FEFF	= Effective scattering amplitude
FMS	= Full multiple scattering
IR	= Infrared spectroscopy
KMITL	= King Mongkut's Institute of Technology Ladkrabang
LCA	= Linear combination analysis
MD	= Molecular dynamics
MM	= Molecular mechanics
NMR	= Nuclear magnetic resonance
QM	= Quantum mechanics
QM/MM	= Quantum mechanics/Molecular mechanics
RDF	= Real space multiple-scattering
RSMS	= Radial distribution function
SCF	= Self-consistent field
SLRI	= Synchrotron Light Research Institute
SPL	= Siam Photon Laboratory
XANES	= X-ray absorption near edge structure
XAS	= X-ray absorption spectroscopy
XES	= Nonresonant x-ray emission

CHAPTER I

INTRODUCTION

In the recent years, advanced material characterization techniques have been invented for studying material properties. The new techniques have been adopted and applied in many disciplines, such as physics, chemistry, biology, medicine and nanotechnology. Base on fundamental solid state physics, the procedures to characterize crystalline materials are well established. It can be stated that, with a few exemptions, the crystals known to human can be classified into seven crystal systems and fourteen Bravais lattices (Marder, 2000). The microscopic structure of crystalline materials can be revealed in atomic resolution by following the well-established procedures. The remarkable successes of diffraction-based techniques (i.e. x-ray, electron, neutron etc.) in the last century have paved the way for new material applications of the present day. For examples: protein crystallography is a major characterization technique in protein study (Caffrey, 2003) while neutron diffraction is very important for magnetic material studies, such as antiferromagnetic material (Shull, 1949).

However, the interpretations of results from above diffraction techniques are mostly based on Fourier transform which require good structural periodicity over a large portion of the materials under study (Bracewell, 2000). Therefore, diffraction techniques may not be used effectively for the structural investigation of materials that (1) do not have periodic structure and are highly disorder (amorphous) or (2) contain randomly distributed components (alloys, dopants in semiconductors, liquid, ions in liquid). For such system, there are other techniques which are capable of

microscopic study, i.e. nuclear magnetic resonance (NMR), infrared spectroscopy (IR) and x-ray absorption spectroscopy (XAS). To use those techniques efficiently, some complementary theoretical models are generally needed. In the recent years, computational simulation have been widely employed and enabled researchers to make structural predictions about the structures of non-crystalline materials. However, to judge the accuracy of any theoretical models, the experimental verification is crucial. Recently, x-ray absorption spectroscopy (Rehr and Albers, 2000) has been shown to be an efficient way to gain structural information of non-crystalline materials when couple experiments with theoretical simulation.

To further explore the capability of XAS for non-crystalline materials, in this thesis, two representative disorder systems (Ca^{2+} in water and zinc oxynitride alloys) are selected for structural study by combining XAS technique with theoretical simulation. In this chapter, the related works published on the two systems are reviewed. The research objectives and scope and limitation of this study are also given at the end of the chapter.

1.1. Background on Ca^{2+} hydration structure

Ca^{2+} is one of the vital ions in biochemical processes throughout human body's fluids such as neuromuscular transmission (Dodge *et al.*, 1967) and hormone secretion (Brown and MacLeod, 2001). In living organism, since water is one of the main chemical components, Ca^{2+} would be found in the form of aqueous solutions or $\text{Ca}^{2+}_{\text{aq}}$. The water polar molecules would arrange themselves around Ca^{2+} resulting in the formation of Ca^{2+} hydration structure. This hydration structure would be the main contributor to govern the transport properties of Ca^{2+} ions throughout living organism.

To understand its behavior in aqueous solution, precise enough for transport modeling, the Ca^{2+} hydration structure must be verified with good accuracy. For theoretical prediction of Ca^{2+} hydration structure, several groups have reported their findings with a variety of results as shown in table 1.1. In this thesis, the main structural parameters of interest are R_0 which is the radius of the first hydration shell or Ca-O distance, σ^2 or Debye-Waller factor which is related to the thermal disordering, and N which is coordination number or the number of water molecules in the first hydration shell.

Table 1.1 Results from theoretical predictions for Ca^{2+} hydration structure: R_0 is nearest neighbor distance, σ^2 is Debye-Waller factor, and N is coordination number.

Type of calculation	R_0 (Å)	σ^2 (Å ²)	N
MD ^a	2.48	0.008	7.9
MD ^b	2.40	0.020	8
MD ^c	2.54	-	9.3
MD ^d	2.45	-	7-8
MD ^e	2.45	0.007	6.5
CPMD ^f	2.45	-	6
QM/MM HF ^g	2.48	-	7.89
QM/MM DFT ^g	2.48	-	8.04

^a(D' Angelo *et al.*, 2004)

^b(Jalilehvand *et al.*, 2001)

^c(Periole *et al.*, 1997)

^d(Bernal-Uruchurtu *et al.*, 1995)

^e(Dang *et al.*, 2006)

^f(Bakó *et al.*, 2002)

^g(Schwenk and Rode, 2004)

It can be seen from table 1.1 that there are some disagreements between different models from theoretical predictions, especially in coordination numbers N , ranging from 6 to 9 and Debye-Waller factor σ^2 ranging widely from 0.008 to 0.02 \AA^2 . It is noteworthy that when dynamic of the structure is considered, the coordination numbers N may not be constant. Figure 1.1 compiles snapshots of the Ca^{2+} hydration structures from some predictions. Clearly, there should be some methods to distinguish “good” model from “not good” model.

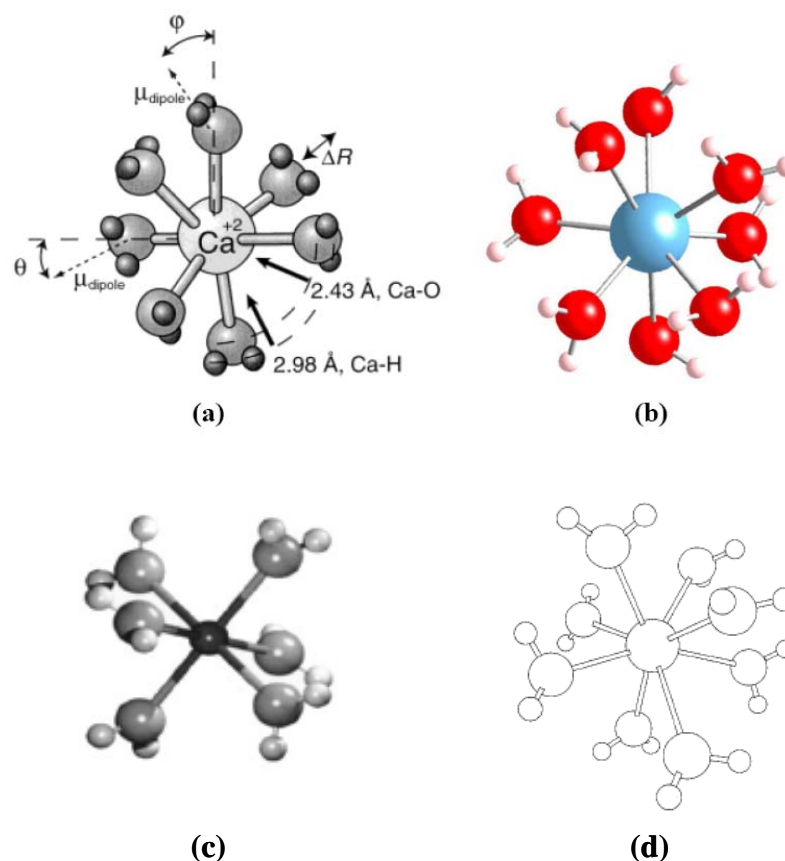


Figure 1.1 Snapshot of first Ca^{2+} hydration shell form (a) (Fulton *et al.*, 2003), (b) Tongraar, (c) (Bakó *et al.*, 2002) and (d) (Jalilehvand *et al.*, 2001)

To verify the predictions of Ca^{2+} hydration structures several experiments have been performed. Neutron diffraction was used to study the environment of Ca^{2+} ion in aqueous solvent (Hewish *et al.*, 1982). It was found that the coordination number decreased from about 10 to 6 with the increase of solution concentration from 1 to 4.5 m. The radius of the first hydration shell was reported to be around 2.46 Å. Other than neutron diffraction, large-angle x-ray scattering study on aqueous calcium halide solutions reported the mean Ca-O bond distance of 2.46 Å and the coordination number of 8 (Jalilehvand *et al.*, 2001).

Fulton *et al.* have experimentally studied the effect of concentration of calcium ion in aqueous using extended x-ray absorption fine structure (EXAFS) and x-ray absorption near edge structure (XANES) (Fulton *et al.*, 2003). They concluded that the mean coordination number was 7.2 ± 1.2 aqueous molecules and the averaged Ca-O distance was 2.437 ± 0.010 Å for 6 m CaCl_2 in water. Recently, Dang *et al.* have reported good agreement between the measured EXAFS spectra and the calculated EXAFS spectra based on their molecular dynamics simulation (Dang *et al.*, 2006). The averaged Ca-O distance was reported to be 2.429 ± 0.03 Å and the coordination number was 6.8. However, the results on XANES measurement have not been discussed. Moreover, there is no reported theoretical model that give the Debye-Waller factor close to the experiment value. In table 1.2, the results from experimental findings are summarized. It could be seen that the disagreements in the values of coordination number and Debye-Waller factor are not solved by experiment yet.

Table 1.2 The main structural parameters of Ca^{2+} hydration structure from various experimental studies

Experimental method	R_0 (Å)	σ^2 (Å ²)	N
	2.46±0.03 (1.0 m)	-	10.0±0.6
Neutron diffraction ^a	2.39±0.02 (2.8 m)	-	7.2±0.2
	2.41±0.03 (4.5 m)	-	6.4±0.3
large-angle x-ray scattering ^b	2.46	0.006	8
EXAFS ^c	2.437±0.010 (6.0 m)	0.011	7.2±1.2
EXAFS ^d	2.429±0.03 (6.0 m)	0.012	6.8

^a(Hewish *et al.*, 1982)
^b(Jalilehvand *et al.*, 2001)
^c(Fulton *et al.*, 2003)
^d(Dang *et al.*, 2006)

Nevertheless, XAS analysis seems to be the alternative method that may possibly give the solution for this kind of structure, since EXAFS and XANES feature is a close dependent of the local structure around the central atom, especially the first shell. The precision of the theoretical model may be evaluated from a comparison between the theoretical and the measured XAS spectra. The possibility of performing XAS experiment using synchrotron radiation helps us to select this method as the main experimental tool for the thesis work.

Therefore, in the first part of this thesis, the verification of the Ca^{2+} hydration structure by XAS is focused. The dynamic configurations data set is provided by Assoc. Prof. Dr. Anan Tongraar, School of Chemistry, Suranaree University of Technology (SUT). A snapshot from the dynamic structure is shown in figure 1.1 (b). Note that, this snapshot has the coordination number of 8. The obtained positions of

atoms are used to generate the calculated XAS spectra. Then the calculated spectra are compared with the measured spectra using the XAS facility at the beamline 8 of the Siam Photon Laboratory, Synchrotron Light Research Institute, Thailand. By this way, the accuracy of the Ca^{2+} hydration model can be verified especially for the value of Debye-Waller factor and coordination number of the first hydration shell.

1.2 Background on Zinc oxynitride alloys

The second part of this thesis is focused on microstructure investigation of zinc oxynitride alloys by using XAS. Because of many of their interesting and useful properties, zinc-contained compounds have widely been studied. For example, zinc oxide has been studied extensively for blue light emitting applications (Murai *et al.*, 2008). Its attractive properties include high transparency and high conductivity (Nanto *et al.*, 1984). For spintronics applications, ZnMnO and ZnCoO alloys are candidates for material of choice. (Kane *et al.*, 2005) In a similar fashion, zinc nitride have been studied and aimed for utilization in optoelectronics applications. The optical band gap of zinc oxide and zinc nitride are found to be around 3.3 eV (Izaki and Omi, 1996) and 1.23 eV (Kuriyama *et al.*, 1993) respectively. Figure 1.2 shows the ball-and-stick models for zinc oxide (a) and zinc nitride crystals (b).

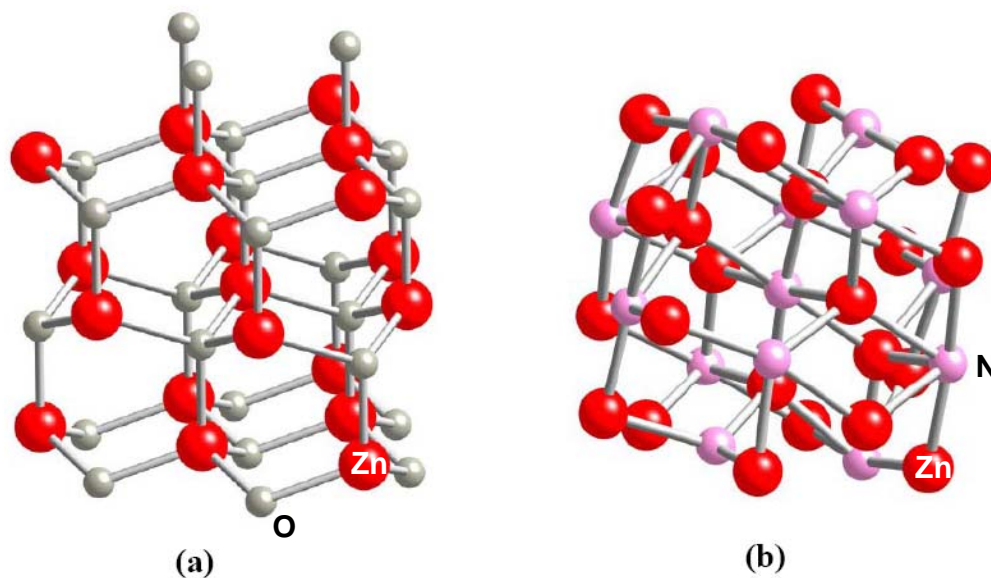


Figure 1.2 Ball-and-stick models for (a) zinc oxide (ZnO) and (b) zinc nitride (Zn₃N₂) crystals.

It has been speculated that the alloys between zinc oxide and zinc nitride or “zinc oxynitride” may have bandgap varying from 1.23 to 3.2 eV, ranging from visible to UV region. Several groups have reported the synthesis of zinc oxynitride alloys and measured the structural and optical properties. M. Futsuhara *et al.* (Futsuhara *et al.*, 1998) used RF sputtering to deposit zinc oxynitride films and found that the optical band gap of their samples could be varied from 2.30 to 3.26 eV with decreasing hydrogen concentration. They conclude that the microstructure of zinc oxynitride film depends on N₂ concentration during the sputtering process. T. Morika *et al.* (Moriga *et al.*, 2005) reported that anti-bixbyite-type zinc oxynitride can be prepared from nitriding zinc powder under ammonia gas flow with varying of nitrogen gas concentration. From the measurement of O K-edge and N K-edge XANES from zinc

oxynitride samples, it has been concluded that nitrogen may be incorporated in octahedral environment in anti-bixbyite zinc oxynitrides.

It should be mentioned that there are some inconsistencies in the work by T. Morika *et al.* such as the difference in nitrogen/oxygen ratio between expected value and composition analysis. Moreover, Zn K-edge XANES spectra has not been measured and phase separation between the two compounds was not considered.

Up to present, there is a limited number of published works on zinc oxynitride alloys and it is unclear about the structure of this kind of alloys as summarized in table 1.3. Therefore, the local structure of zinc oxynitride alloys is, for the most part, unknown and waiting to be solved. Moreover, by comparing to indium oxynitride alloys studied by J. T-Thienprasert *et al.* (Thienprasert *et al.*, 2008), it is possible that zinc oxynitride alloys may have disorder structure. Therefore, we selected to study the local structure of zinc oxynitride alloys by XANES in the second part of the thesis.

Table 1.3 Results from experimental studies of zinc oxynitride

Synthesis technique	Compositions	Structure	Bandgap (eV)
RF sputtering ^a	Zn _x N _y O _z	Zincblend (XRD)	2.30-3.26
Nitridation ^b	Zn ₃ (N _{1-x} O _x) _{2-y}	Anti bixbyite (XRD)	-

^a(Futsuhara *et al.*, 1998)

^b(Moriga *et al.*, 2005)

In this work, several candidate models for zinc oxynitride were considered. Theoretical XANES spectra were generated. The verification of the theoretical spectra is done by comparing with the actual measurement by using zinc oxynitride samples

supplied by Prof. Jiti Nukaew's research group of King Mongkut's Institute of Technology Ladkrabang (KMITL), Thailand.

1.3 Research objectives

(a) Verify the validity of a Ca^{2+} hydration QM/MM model by comparing the calculated spectra with the measured spectra and extract the important structural parameters for $\text{Ca}^{2+}_{\text{aq}}$ from XAS fitting

(b) Study the local structure of zinc oxynitride thin films by XANES technique and propose a general scheme for XAS study of non-crystalline material.

1.4 Scope and limitation of the study

The calculated x-ray absorption spectra are based on FEFF 8.2 code (Ankudinov *et al.*, 1998). To verify the dynamically simulated Ca^{2+} hydration structure by Assoc. Prof. Dr. Anan Tongraar, both XANES and EXAFS spectra are calculated and compared with experimental XAS data taken at the synchrotron radiation facility of the Siam Photon Laboratory (SPL), Nakhon Ratchasima, in the first half of this thesis work. In the second half, the local structure of zinc oxide/zinc nitride alloys is studied by XANES approach. The zinc oxynitride thin films are prepared by KMITL group. The XAS experiment is performed at SPL as well. To be compared with the measurement, Zn K-edge XANES spectra were generated from several configuration models. A representative model of zinc oxynitride local structure will be selected from the model that gives the best fit.

CHAPTER II

RESEARCH METHODOLOGY

In this chapter, the research methodology used in this thesis will be reviewed. Firstly, the basic theory on x-ray absorption spectroscopy (XAS) is discussed. Secondly, the XAS measurement facility at Synchrotron Light Research Institute (SLRI) is introduced. Then, the details of the XAS spectrum calculation and XAS spectrum analysis will be discussed in the following section. Finally, the background information about Ca^{2+} hydration QM/MM simulation for this study and zinc oxynitride alloys modeling will be discussed in the last section.

2.1. X-ray absorption spectroscopy

X-ray absorption spectroscopy (XAS) is one of the techniques used widely in the investigation of microscopic and electronic structure of materials. The experiment is usually performed at the synchrotron radiation facility, where the energy of x-ray photon can be varied and selected. This technique measures the x-ray absorption coefficient of the absorbing material as a function of x-ray photon energy, covering the range around the absorption edge of absorbing atoms of interest.

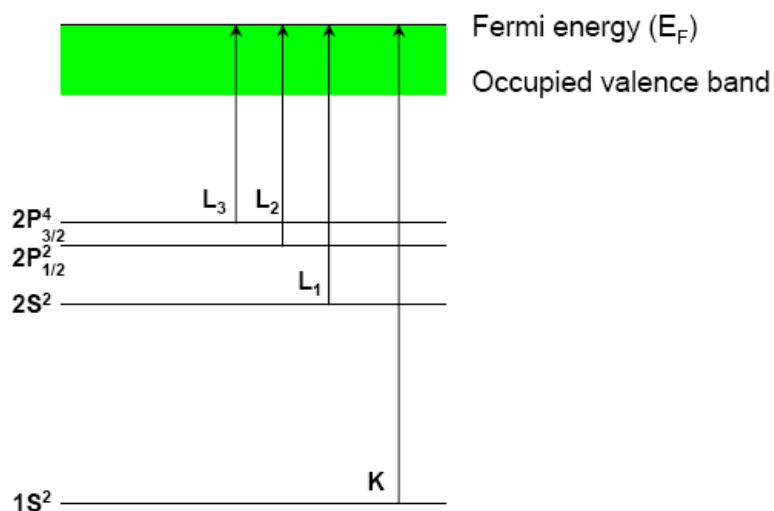


Figure 2.1 The relationship between the x-ray absorption edges and the corresponding excitation of core electrons. Shown are the excitations corresponding to the K, and L x-ray absorption edges.

In the absorption process, electrons in the inner shells: K, L or M shell will be excited by the (absorbed) x-ray photon to higher empty energy states above the Fermi energy. The core hole, empty state, will be created in the inner shell, and the energy level of the shell is used to define the type of absorption edge as shown in figure 2.1. For example, K-edge is the absorption edge when the excited electrons are from 1s shell and L_1 -edge is the absorption edge when the excited electrons are from 2s shell. The x-ray photon energy has to be greater than the difference of energy between unoccupied valence state and K shell state. At the photon energy above the binding energy, the absorption rapidly change, which is obviously seen as the absorption edge. For example, shown in figure 2.2 is the measured K-edge absorption spectrum of Ca^{2+}_{aq} from 6 M $CaCl_2$ aqueous solution.

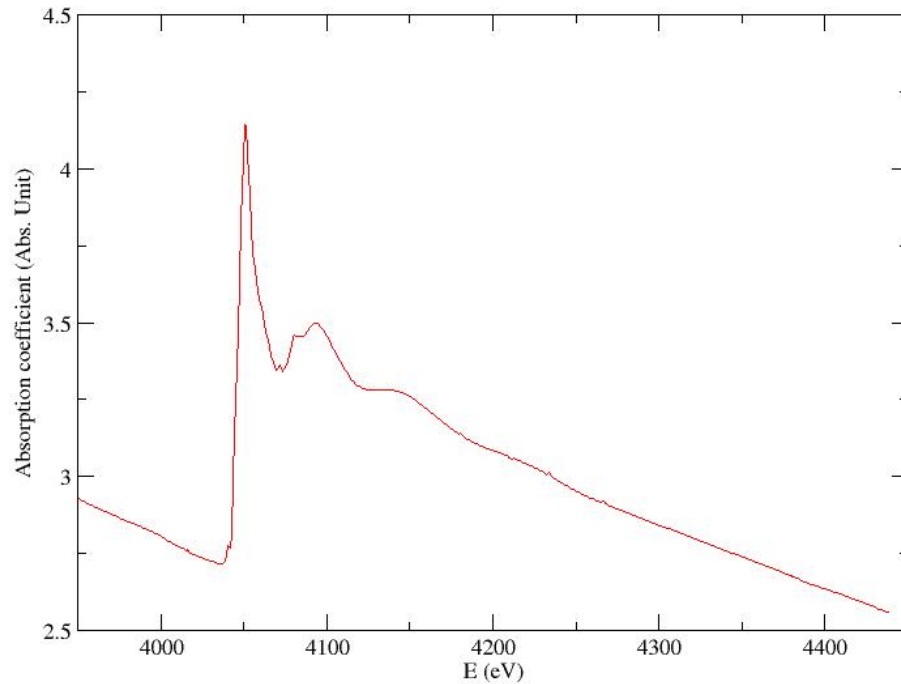


Figure 2.2 K-edge raw absorption spectra of $\text{Ca}^{2+}_{\text{aq}}$ from 6 M CaCl_2 aqueous solution: data taken at XAS beamline, Siam Photon Laboratory.

The absorption ability is studied through the absorption coefficient (μ) as a relation of the intensity of incident beam (I_0) and the intensity of transmitted beam (I) as defined by

$$I = I_0 e^{-\mu x} , \quad (2.1)$$

where x is the thickness of the sample, which is generally can be abandoned in the standard data analysis as some scaling constant.

Generally, the absorption spectrum can be separated into two regions: x-ray absorption near edge structure (XANES) and extended x-ray absorption fine structure (EXAFS). Because of the continuity of absorption spectrum, the regions of XANES and EXAFS can be overlapped and hardly defined at the beginning and the end of two

regions. However, it is generally defined that XANES locates at around 40-50 eV above the absorption edge and EXAFS locates at the higher energy region as show in figure 2.3.

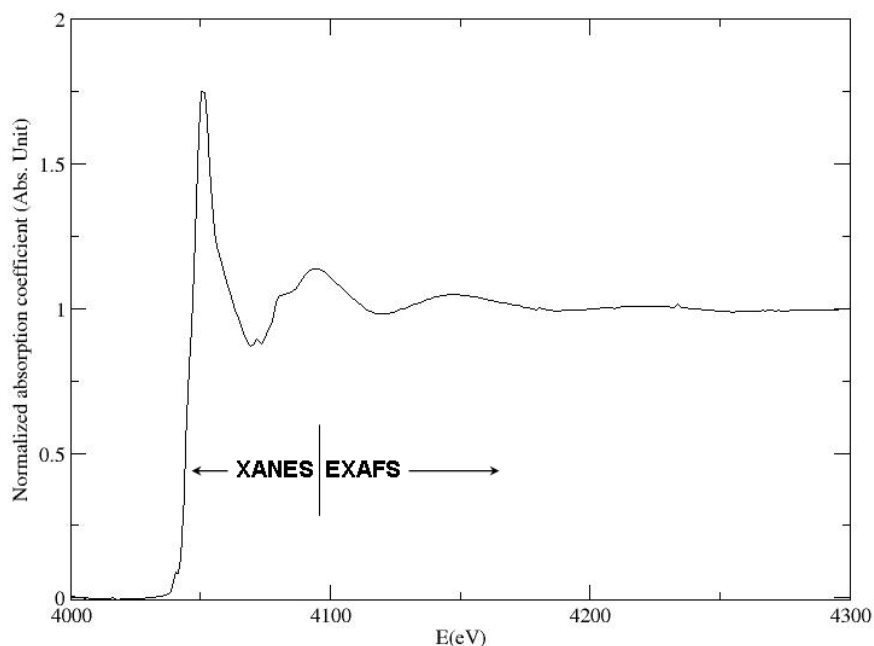


Figure 2.3 Normalized K-edge absorption spectrum can be classified into two regions, XANES and EXAFS. Data shown is the XAS spectrum of $\text{Ca}^{2+}_{\text{aq}}$.

2.1.1 X-ray absorption near-edge structure (XANES)

XANES spectrum is known to be sensitive to the local environment and the oxidation state around the absorbing atom. Considering an excited electron, which has low energy in this region, like a wave, it will go out from the absorbing atom and scatter from a number of surrounding atoms before going back to the absorbing atom. This phenomenon is sensitive to the arrangement of neighboring atoms and also effects to the absorbance which can be measured. Therefore, XANES is usually used to study the oxidation state and the local orientation of material.

The expression for XANES can be derived from the transition rate given by Fermi's Golden Rule. The absorption coefficient in equation (2.1) can be described by

$$\mu(E) \propto \sum_f |\langle f | \hat{\epsilon} \cdot \hat{r} | i \rangle|^2 \delta(E_i - E_f + \hbar \omega), \quad (2.2)$$

where $|i\rangle$ is the initial core *ket* state vector, $\langle f|$ is the final *bra* state vector of the excited electron, E is the energy of absorbed x-ray photon, E_i is the energy of final state, E_f is the energy of final state, $\hbar \omega$ is the energy of x-ray photon energy, $\hat{\epsilon}$ is the x-ray polarization vector and $\mu(E)$ is absorption coefficient with ignoring of core-hole lifetime and experimental resolution (Ankudinov et al., 1998). By considering Eq. 2.2 further with the additional effects of core-hole life time and experimental resolution, the XANES spectra can be calculated as described later in section 2.3.2.

2.1.2 Extended x-ray absorption fine structure (EXAFS)

EXAFS is the oscillatory modulation of absorption coefficient which can be inspected in the higher energy part of absorption spectrum. This fine structure occurs from interacting of excited electrons with absorbing atom and its surroundings, which affect directly to the absorbance. In quantum mechanical aspect, the photoelectron is treated as wave emitted from the absorber with wavelength equal to λ , which can be defined by the de Broglie relation

$$\lambda = \frac{h}{p}, \quad (2.3)$$

where h is Planck's constant and p is the momentum gained by photoelectron. In EXAFS, p is related to equation described the free electron

$$\frac{p^2}{2m} = \hbar \omega - E_0, \quad (2.4)$$

when m is mass of that excited electron, $h\nu$ is the energy of frequency ν photon and E_0 is the binding energy of the core level electron.

Consider a Zn K-edge absorption spectrum from ZnO sample as shown in figure 2.4, the wave form of outgoing photoelectron from an absorbing atom (Zn) and the backscattered waves from surrounding atoms (O) will interfere and then create the total amplitude. The total amplitude of electron wave function would be magnified or declined depends on phase difference of these two kinds of considered waves. The amplitude will be magnified and detected as peak of fine structure, if they are exactly in phase. On the other hand, the amplitude will be declined and detected as valley of fine structure, if they are out of phase.

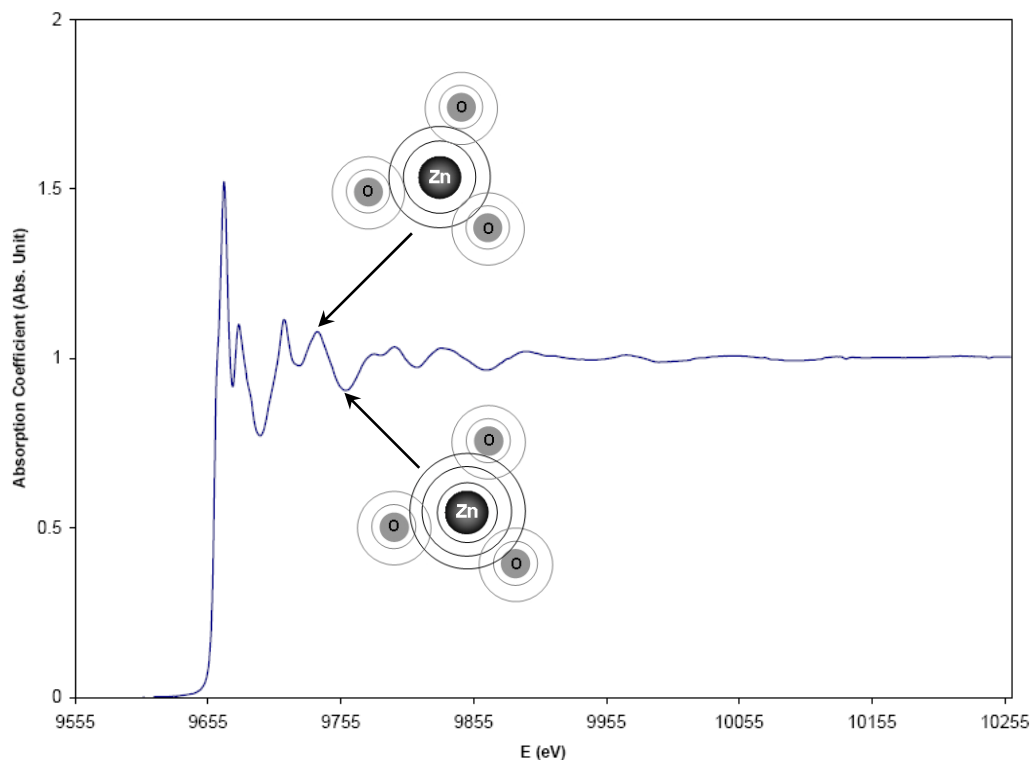


Figure 2.4 Result from the interaction of electron out-going wave from Zn absorber in ZnO and its surrounding O atoms in EXAFS region.

Noting that, the fine structure in EXAFS does not present in the case of isolate atom system such as mono-atomic gas, because the outgoing wave would not be scattered strongly by any other atoms. In such case, only atomic absorption background is present in the XAS spectrum.

The oscillation of x-ray absorption above a given absorption edge, EXAFS function, $\chi(E)$ is defined as

$$\chi(E) = \frac{[\mu(E) - \mu_0(E)]}{\Delta\mu_0}, \quad (2.3)$$

where $\mu(E)$ is the x-ray absorption coefficient, $\mu_0(E)$ is smooth atomic background absorption coefficient and $\Delta\mu_0$ is a normalization factor as illustrated in figure 2.5.

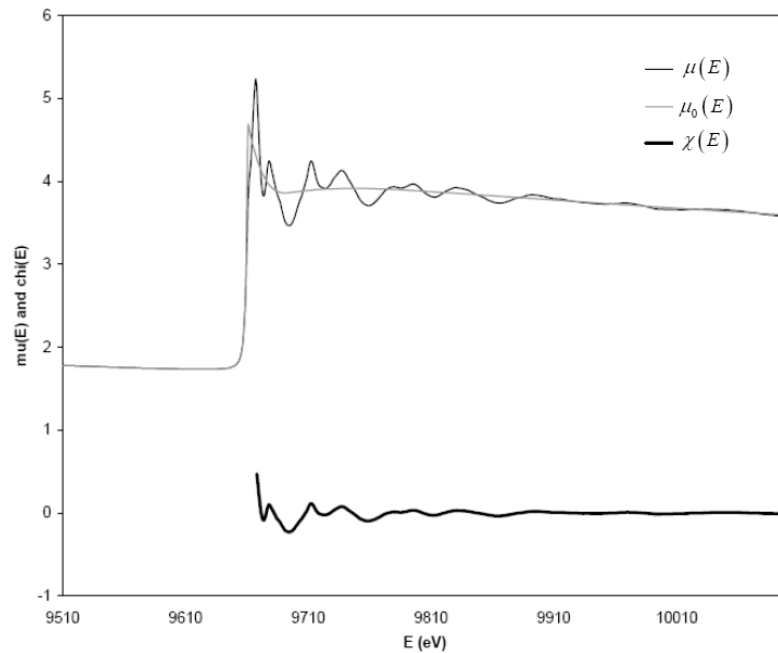


Figure 2.5 The x-ray absorption coefficient $\mu(E)$, the smooth atomic-like background $\mu_0(E)$ and EXAFS function $\chi(E)$ for Zn-K edge spectrum of ZnO.

Moreover, in the EXAFS analysis $\chi(E)$ could be changed from E space to k space by the relation $k = \sqrt{2m(E - E_0)/\hbar^2}$. Then the function can be changed from $\chi(E)$ to $\chi(k)$ for general purpose. In theoretical approach, the $\chi(k)$ can be expressed by (Wilson *et al.*, 2000)

$$\chi(k) = \sum_j \frac{S_o^2 N_j}{k R_j^2} |f_j(k, \pi)| \sin[2kR_j + \phi_j(k)] e^{-2\delta_j^2 k^2} e^{-2R_j/\lambda(k)}, \quad (2.4)$$

where N_j is the number of neighbors in j shell of surrounding atoms, k is photoelectron wave vector, f_j is the scattering amplitude, $S_o^2(k)$ is the amplitude reduction term due to many-body effect, R_j is radial distance from absorbing atom to j shell, $\lambda(k)$ is electron mean free path, σ_j is the Debye-Waller factor and $\phi(k)$ accounts for the total phase shift of the curve wave scattering amplitude along the scattering trajectory.

The distance between center atom and backscattering atoms or the path-length change the phase varying with the wavelength of photoelectron. In addition, different types of surrounding atoms vary the backscattering strength as a function of photoelectron energy. It is accepted that, by the careful analysis of the EXAFS structure, one can obtain important structural parameters surrounding the center atom.

2.2 X-ray absorption spectroscopy experimental set up

The x-ray absorption spectroscopy experiment is normally performed at a synchrotron radiation source, because of high intensity and energy adjustable ability of produced x-ray photon, and the ability to obtain the continuous absorption spectrum over wide energy range. In general, there are three types of x-ray absorption

measurements: transmission-mode XAS, fluorescence-mode XAS and electron-yield XAS as diagrammatically shown in figure 2.6.

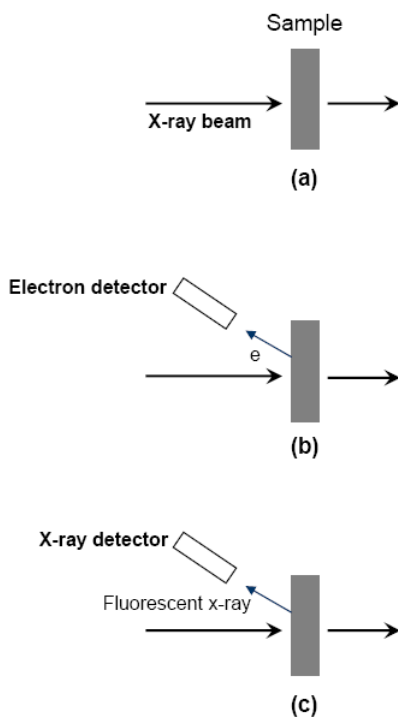


Figure 2.6 Three modes of XAS measurement; (a) transmission mode, (b) electron yield and (c) fluorescence mode.

In the transmission-mode XAS, after the energy of x-ray photons being adjusted by monochromator, the intensities of incident x-ray photon beam (I_0) and the transmitted x-ray photon beam (I) are measure by ionization chambers as shown in figure 2.7. The absorption coefficient can be extracted based on equation (2.1). The actual experimental set up of XAS experimental station at XAS beamline, Siam Photon Laboratory, SLRI is shown in figure 2.8.

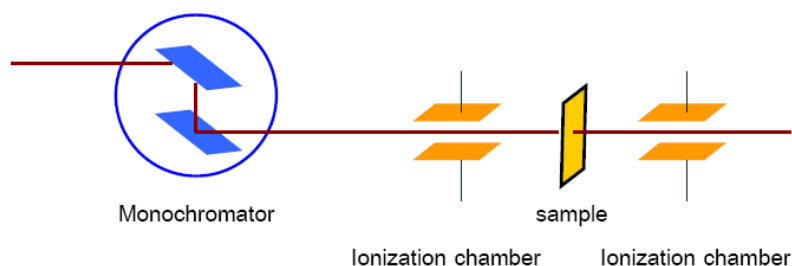


Figure 2.7 Schematic illustration of the experimental setup of transmission-mode x-ray absorption spectroscopy

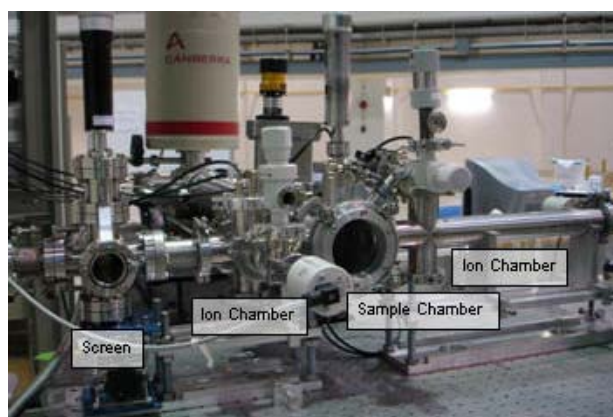


Figure 2.8 XAS experimental set up at the Siam Photon Laboratory, Synchrotron Light Research Institute.

Apart from the transmission mode, the fluorescence mode and the electron yield are also capable for the measurement of the absorption coefficient. In the x-ray absorption phenomena, where the electrons in higher energy level fill the hole left by the excited electron, the defined energy x-ray photon will be released as illustrated in figure 2.9 (a) and the fluorescence x-ray can be detected. Furthermore, de-excitation can cause the Auger effect, where the electron drops to lower energy state, a second

electron can be excited to the continuum state and possibly go out from the sample as shown in figure 2.9 (b), and then it can be detected by electron-yield XAS detectors. However, both processes are directly proportional to the absorption ability of the sample. Therefore, the three techniques are capable for the study of the structure of material using the absorption ability of the sample.

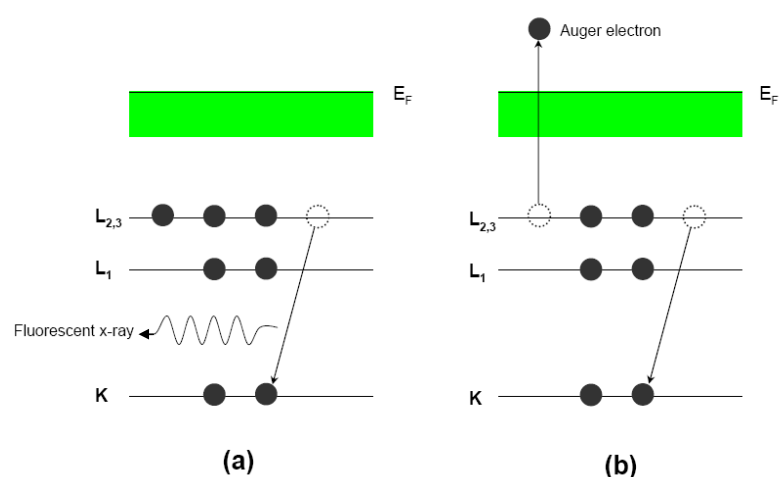


Figure 2.9 The excited state (a) x-ray fluorescence and (b) the Auger effect.

2.3 X-ray absorption spectrum calculation

2.3.1 FEFF code overview

In this thesis, the main theoretical calculations are approached on FEFF 8.2 code. This code is one of developed codes to mainly calculate x-ray absorption spectra for the FEFF project developed by the Department of Physics, University of Washington, Seattle, USA. FEFF code is written in ANSI FORTRAN 77 with principal investigator John J. Rehr and co-principle investigator Alexei L. Ankudinov. The name "FEFF" refers to the effective scattering amplitude f_{eff} . Other than XAS spectra

calculation, FEFF code can calculate x-ray magnetic and natural circular dichroism, nonresonant x-ray emission (XES) and electronic structure including local density of states (LDOS).

FEFF is *ab initio* self-consistent real space multiple-scattering (RSMS) formalism code for simultaneous calculations of x-ray-absorption spectra and electronic structure. The properly edited input file “feff.inp” will be calculated by various modules, which can be used as standard options, useful option or advanced option.

The commands, parameters and atomic positions for FEFF-XAS spectrum calculations can be edited within the input file named “feff.inp”, which is shown in figure 2.10. This file is headed with some details, such as the generator of input file and contained atoms in the cluster. The followed details are about many cards used to define the steps of calculation. The types of atomic potentials and defined atomic symbols are shown in the next part, and finally with the positions of all generated atoms in the system where the position of center atom is located at (0,0,0) in (x,y,z) coordination.

The crystal structure described in “feff.inp” can be generated directly from ATOMS code via “atoms.inp” as shown in figure 2.11. To create “feff.inp” from “atoms.inp” is optional and capable only for periodic structure. However, the atomic position in disorder system can be modified directly within “feff.inp” itself as used in Ca^{2+} hydration system.

```

* This feff.inp file generated by ATOMS, version 2.50
* ATOMS written by and copyright (c) Bruce Ravel, 1992-1999

* -- * -- * -- * -- * -- * -- * -- * -- * -- * -- * -- * -- * -- * -- *
*      total mu =      1206.4 cm^-1, delta mu =      1030.4 cm^-1      *
*      specific gravity = 5.690, cluster contains 340 atoms.        *
* -- * -- * -- * -- * -- * -- * -- * -- * -- * -- * -- * -- * -- *
*      mcmaster corrections: 0.00049 ang^2 and 0.433E-06 ang^4      *
* -- * -- * -- * -- * -- * -- * -- * -- * -- * -- * -- * -- * -- *

TITLE      ZnO

EDGE       K
S02        1.0

*          pot      xsph  fms   paths genfmt ff2chi
CONTROL    1        1      1     1     1     1
PRINT      1        0      0     0     0     0

*          r_scf   [ l_scf  n_scf  ca ]
SCF        6.00    0       15    0.1

*          ixc    [ Vr  Vi ]
EXCHANGE   0      0      0

*EXAFS
*RPATH      8.57378

*          kmax   [ delta_k  delta_e ]
XANES      4.0    0.07    0.5
*          r_fms   [ l_fms ]
FMS        7.00    0
*
RPATH      0.10000
*          emin   emax   resolution
*LDOS      -20    20    0.1

POTENTIALS
*          ipot   z [ label   l_scm  l_fms  stoichiometry ]
           0     30   Zn     -1     -1     0
           1     8    O      -1     -1     1
           2     30   Zn     -1     -1     1

ATOMS
0.00000    0.00000    0.00000    0   Zn    0.00000
0.00000    0.00000    1.94859    1   O    1.94859
-1.87521    0.00000   -0.65091    1   O    1.98497
0.93764    1.62400   -0.65092    1   O    1.98500
0.93764   -1.62400   -0.65092    1   O    1.98500
0.93764    1.62400    2.59950    2   Zn    3.20530
0.93764   -1.62400   -2.59950    2   Zn    3.20530
          :
          :
9.37619   -3.24800   -0.65092    1   O    9.94415
9.37619    3.24800   -0.65092    1   O    9.94415
-7.50092   -6.49600   -0.65091    1   O    9.94412
-7.50092    6.49600   -0.65091    1   O    9.94412

END

```

Figure 2.10 Detail of “feff.inp” input file of ZnO with Zn as center atom for FEFF calculation.

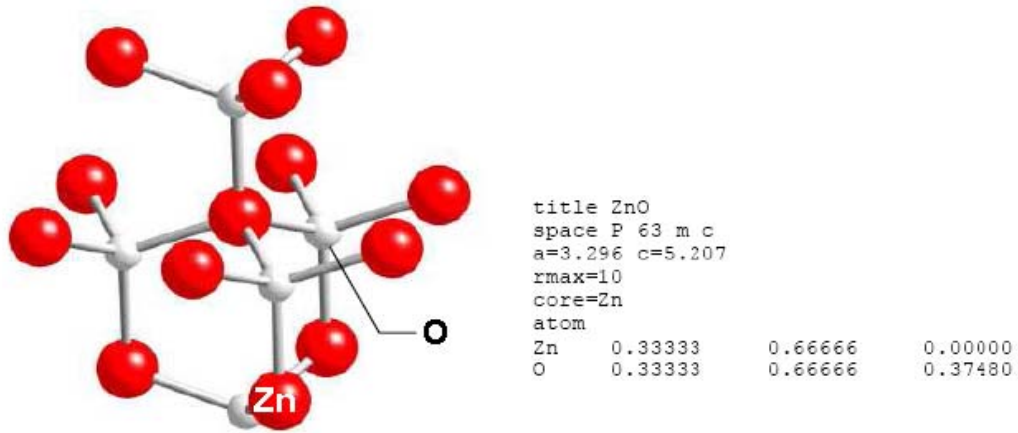


Figure 2.11 Detail of atoms.inp input file to generate “feff.inp” for FEFF calculation.

2.3.2 XAS calculation

XAS calculation can be carried out with the imaginary part of one-electron Green’s function operator (Ankudinov, 1998)

$$G = [E - H]^{-1}, \quad (2.5)$$

where H is the effective one-electron Hamiltonian and E is the photoelectron energy. Based on the Green’s-function calculation in the complex plane, to express Eq. (2.2) by using spectral representation with Green-function operator, Eq. (2.5) becomes

$$\mu(E) \propto -\frac{2}{\pi} \text{Im} \langle i | \hat{\varepsilon} \cdot \hat{r}' G(\hat{r}', \hat{r}, E) \hat{\varepsilon} \cdot \hat{r} | i \rangle, \quad (2.6)$$

where $G(\hat{r}', \hat{r}, E) = \langle \hat{r}' | G(E + i\eta) | \hat{r} \rangle$, $\hat{\varepsilon}$ is the x-ray polarization vector and the parameters denoted with prime is that quantity in final state (Ankudinov, 1998). In addition, since only the transition to unoccupied state above Fermi energy are capable

and the impact of core-hole lifetime and experimental resolution are essentially taken into account, the total coefficient should become

$$\mu(E) = \int_{E_F}^{\infty} dE' \rho(E') \frac{\Gamma}{\pi \left[(E - E')^2 + \Gamma^2 \right]}, \quad (2.7)$$

where Γ is determined by the combination of the core-hole lifetime and experimental resolution, and E_F is Fermi level energy. FEFF code assists scientist to approach the XAS spectra by performing the possibly accurate Green's function in $\rho(E)$. The developers introduced two main developed features for FEFF 8 series to achieve this difficult chore. The two main advantages are the approaches of self-consistent field (SCF) and full multiple scattering (FMS).

Within RSMS Green's-function framework, SCF loops are used to create the SCF potential, muffin-tin potentials, for XAS calculation (especially XANES) after obtaining the total electronic density and Coulomb potential as illustrated in figure 2.12. Muffin-tin potential considers the atomic interval potential as a scattering potential centered on each atom equal to the sum of overlapping potentials and has a constant value in the interstitial region between atoms. FMS card will perform the calculation for all possible paths within the defined cluster.

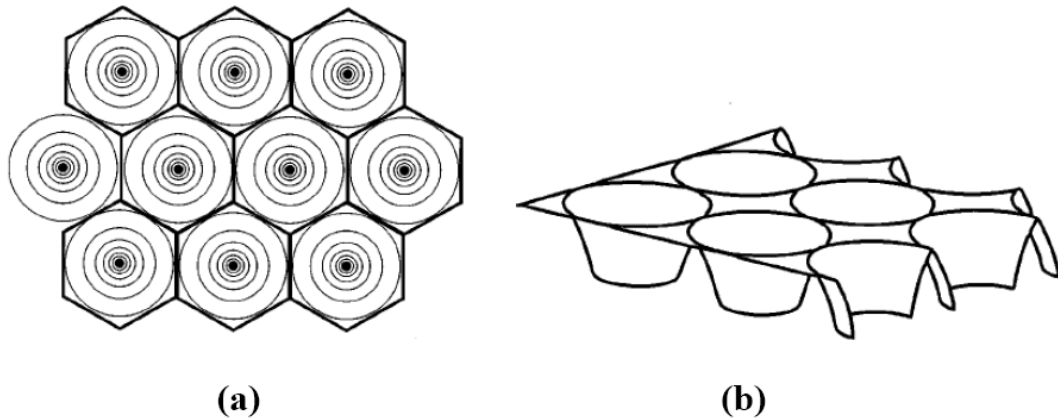


Figure 2.12 Schematic illustration of muffin-tin potential in two dimensions (Rehr and Albers, 2000)

The SCF loop constructs Green's function, which consists of central atom and scattering contribution

$$G(\vec{r}, \vec{r}', E) = G^C(\vec{r}, \vec{r}', E) + G^{SC}(\vec{r}, \vec{r}', E), \quad (2.8)$$

where $G^C(\vec{r}, \vec{r}', E)$ and $G^{SC}(\vec{r}, \vec{r}', E)$ are central atom and scattering contribution respectively.

XANES calculation will be operated under the defined control cards, most of them are usually used as the defaults, excepting FMS and SCF which are essentially cared. To approach the suitable scattering potential form SCF, it should be carefully defined for the cluster radius for SCF consideration, which usually needs around 30 atoms within the cluster. That cluster radius should be defined at the consistent of calculated absorption spectra as shown in figure 2.13. The good SCF cluster should be the least value that makes the consistent of the spectra presents for saving the computational resources.

Similar to the SCF, FMS calculation should be adjusted carefully for the cluster radius for FMS consideration as shown in figure 2.14. In addition, there are other parameters that can be modified for more satisfied spectra, such as the step size of energy.

For EXAFS calculation, the scattering muffin-tin potential has less effect to the calculated spectra than at the lower energy region. At EXAFS region, the photoelectron gain larger energy, and then it is less sensitive to the details of potential between atoms. Therefore, we conclude that SCF calculation may not be necessary in the EXAFS calculation in this work.

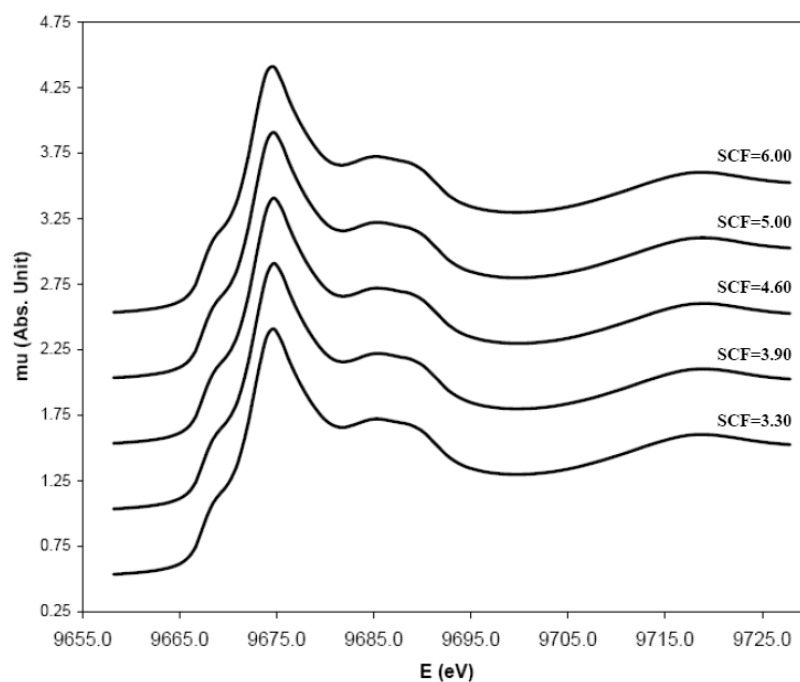


Figure 2.13 Calculated Zn K-edge XANES of ZnO with different SCF parameters

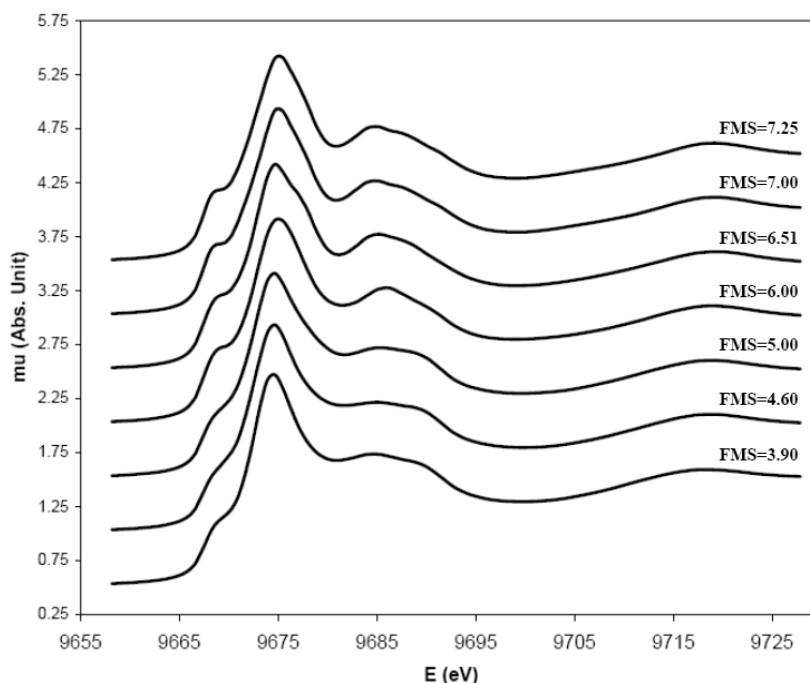


Figure 2.14 Calculated Zn K-edge XANES of ZnO with different FMS parameters

2.4 X-ray absorption spectroscopy spectra analysis

XAS spectra from both experiment and calculation are compared and analyzed by *IFEFFIT* package (Ravel and Newville, 2005). The numerical XAS algorithm in this package was written in the Perl programming language and *Perl/Tk* graphics toolkit. It is the free software developed primarily by Matt Newville at the Consortium for Advanced Radiation Sources, University of Chicago, (CARS), with some borrowing idea and software from UWXAFS Project, University of Washington. In addition, this package includes many ideas of XAS analysis, such as Fast Fourier Transform and non-linear least-squares fitting. For spectrum analysis in this study two programs in the package are used: (1) *ATHENA*, a program for basic XAS spectrum analysis, (2) *ATHEMIS*, a program for EXAFS analysis and fitting the experimental spectra with *FEFF* theoretical modeling.

To obtain the normalized XAS spectra from raw absorption data, some procedure must be performed. The procedure can be outlined as follows:

1. Subtract a smooth pre-edge with proper function.
2. Identify the value of threshold energy.
3. Normalize absorption spectra ($\mu(E)$). The XANES spectrum can be extracted at this step.
4. Change absorption coefficient from a function of photon energy ($\mu(E)$) to wave number ($\mu(k)$).
5. Magnify the fine structure at the higher energy part of EXAFS region by multiplying with k factor.
6. Carry out the Fourier transform to the fine structure from k space to R space.
7. Approach the EXAFS parameters with parameter fitting.

The 1-6 steps are done with *ATHENA* where the last step is done in *ATHEMIS*.

To begin the spectrum analysis, the measured absorption spectrum have to be subtracted by the instrumental background as shown in figure 2.15.

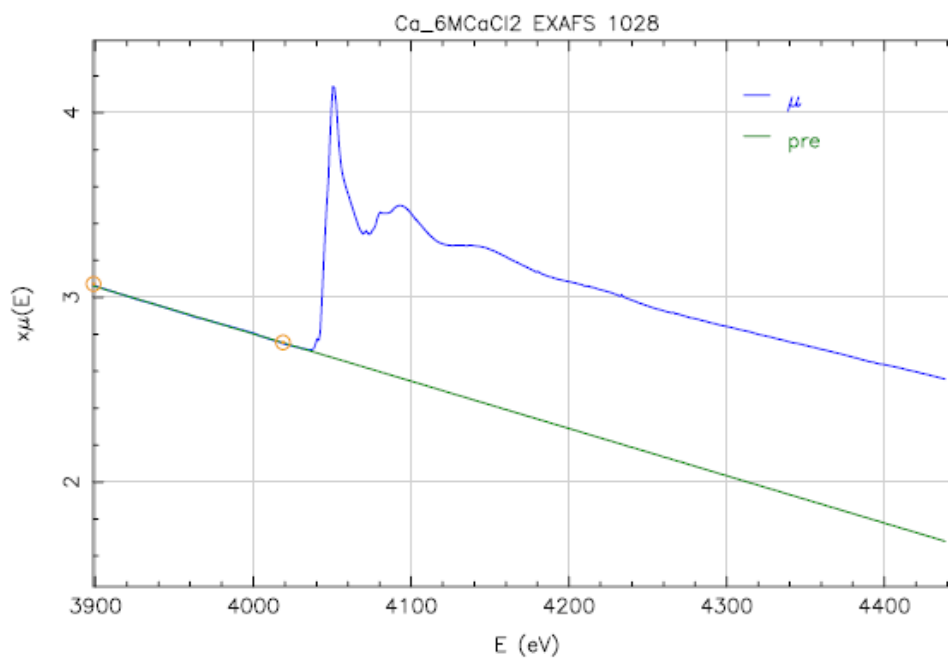


Figure 2.15 Pre-edge background subtractions for measured $\text{Ca}^{2+}_{\text{aq}}$ K-edge XAS spectrum.

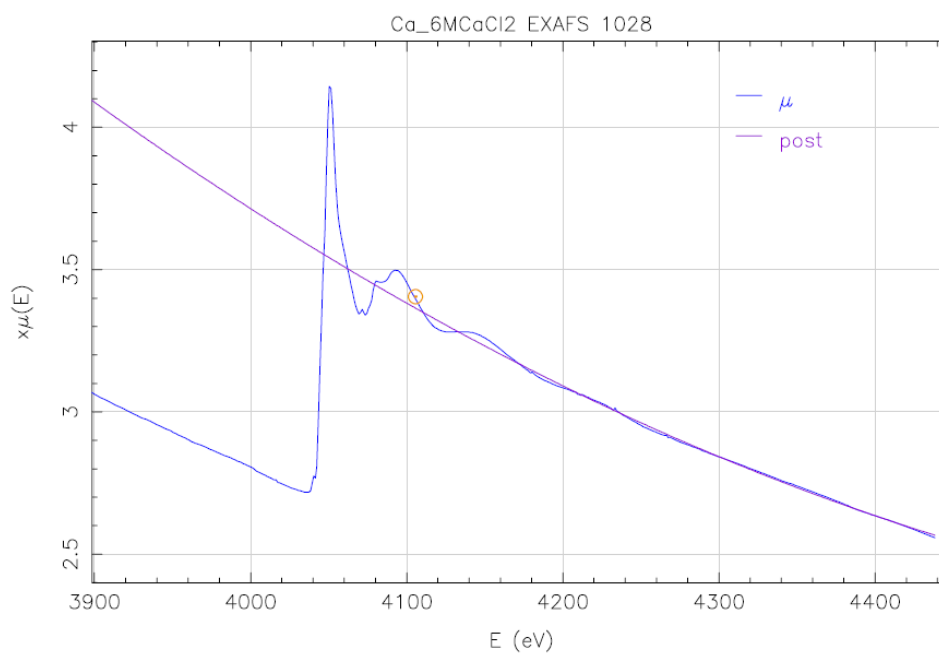


Figure 2.16 Post-edge line or normalization line for measured $\text{Ca}^{2+}_{\text{aq}}$ K-edge XAS spectrum.

After that, to normalize absorption spectra, the normalization rank has to be modified to have a suitable normalization line as shown in figure 2.16. The normalization line is considered as a smooth atomic background absorption coefficient or $\mu_0(E)$ in Eq. 2.3. In fact, $\mu_0(E)$ is the absorption coefficient of isolated atom, however, if there is no actual measurement of isolated atom, the $\mu_0(E)$ can be defined directly but carefully. Nonetheless, the defined $\mu_0(E)$ or normalization line should be a line that makes good fluctuation of EXAFS fine structure. Then, the normalized spectrum is ready as shown in figure 2.17.

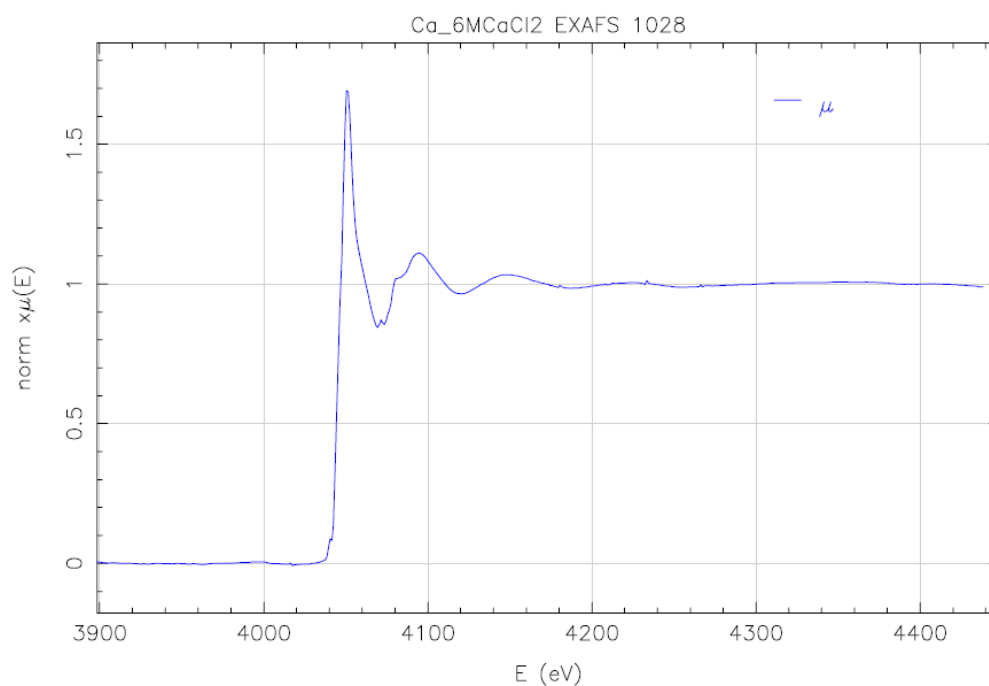


Figure 2.17 Normalized K-edge XAS spectrum for $\text{Ca}^{2+}_{\text{aq}}$

The normalized absorption spectrum for Ca^{2+} K-edge XAS spectrum in XANES region is ready to be compared. However, for EXAFS analysis and fitting, there are some procedures to be carried out further to find the structural parameters, such as R_0 (nearest neighbor distance), σ^2 (Debye-Waller factor), and N (coordination number).

Specifically for EXAFS region, with the expression

$$k = \sqrt{\frac{2m(E - E_0)}{h^2}}, \quad (2.9)$$

where k is wave number ($k = \frac{2\pi}{\lambda}$, where λ is wavelength of photoelectron) and h is Planck's constant divided with 2π , the absorption coefficient $\mu(E)$ will be changed to $\chi(k)$, as shown in figure 2.18.

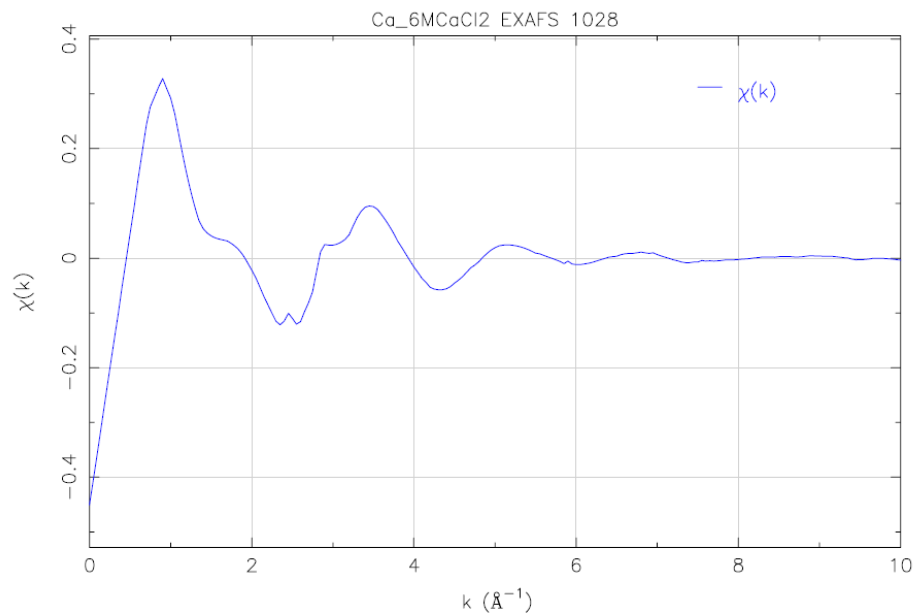


Figure 2.18 K-edge EXAFS spectrum in k space, $\chi(k)$ for $\text{Ca}^{2+}_{\text{aq}}$

EXAFS in k space is usually multiplied with k factor to magnify the fine structure in the higher energy region. In this study, k^2 is used as the multiplication factor for $\chi(k)$, and the $k^2 \cdot \chi(k)$ spectrum is shown in figure 2.19.

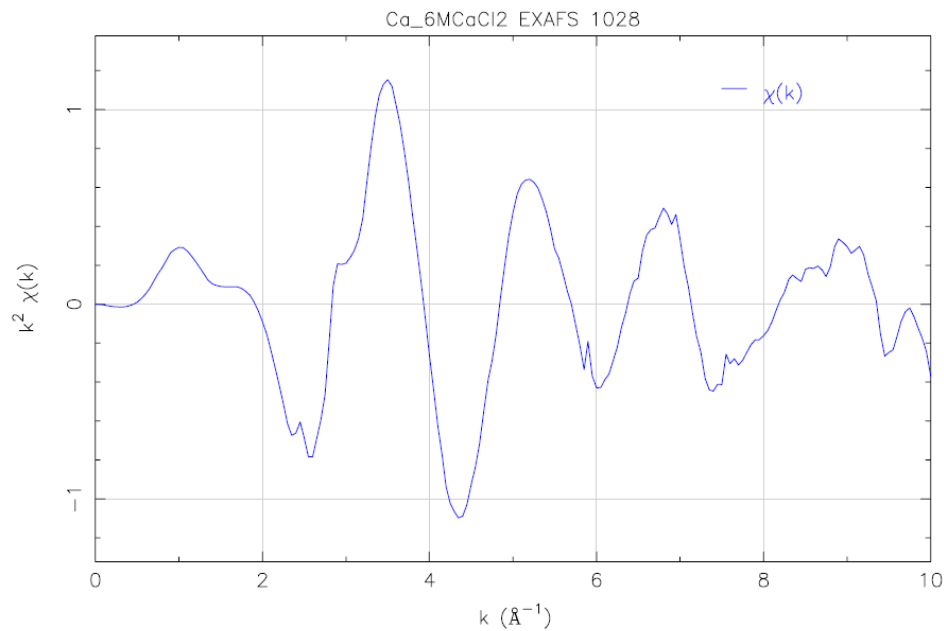


Figure 2.19 k^2 -weighted K-edge EXAFS spectrum for $\text{Ca}^{2+}_{\text{aq}}$

Then, the spectrum in figure 2.19 is transformed from k -space to R -space by Fourier transform for radial environmental analysis. However, before performing the transform, the region of interest may be windowing as shown in figure 2.20. There are a few types of window that can be chose, such as Hanning window, Kaiser-bessel window, Welch window and Parzen window. In this study, the Hanning window $W(k)$, is used. In addition, to get averaged $\chi(R)$ ($\chi^{\circ}(R)$), with $W(k)$ window, the Fourier transform will be performed using the expression (Rehr *et al.*, 1995)

$$\chi^{\circ}(R) = \frac{1}{\sqrt{2\pi}} \int_0^{\infty} k \chi(k) W(k) e^{i2kR} dk, \quad (2.10)$$

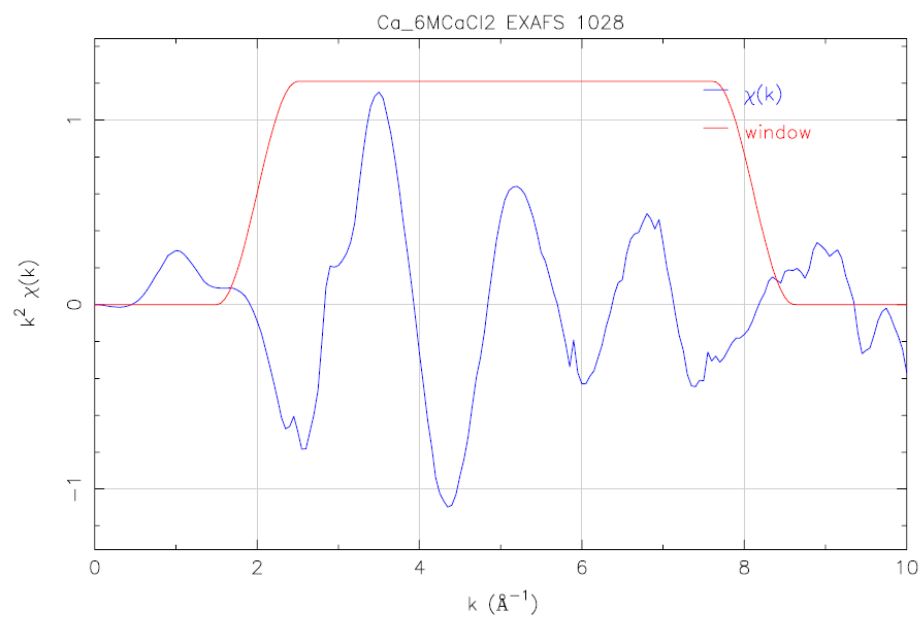


Figure 2.20 k^2 -weighted K-edge EXAFS for $\text{Ca}^{2+}_{\text{aq}}$ with Hamming window

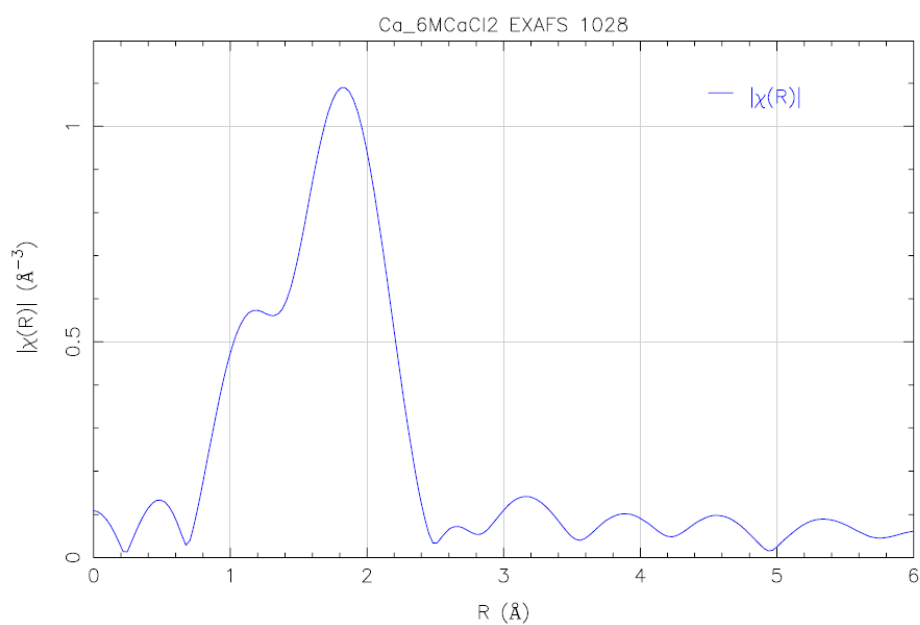


Figure 2.21 K-edge EXAFS spectrum in real space $\chi(R)$ for $\text{Ca}^{2+}_{\text{aq}}$

After performing of Fourier transform, EXAFS spectrum is changed from representation in k-space to R-space as shown in figure 2.21. EXAFS in R-space can be considered as a radial distribution function, which shows the probability of finding any atoms/molecules in any radius from a center atom (shell to shell distance). Then a comparison for measured and calculated EXAFS can be done conveniently in R-space.

For EXAFS fitting, the spectra in k-space would be analyzed further with *ATHEMIS*. The results from data fitting of EXAFS experiments done in this thesis work will be shown in the CHAPTER III.

Linear combination analysis (LCA) is another important utility in *ATHENA* software. In LCA, it can be assumed that XANES of one unknown sample can be fitted by the combinations of any pure references. Any XANES compositions can be combined to be fitted with the unknown XANES spectrum. The better or worse fitting can be judged by R-factor defined by

$$R - factor = \frac{\sum (XANES_{MEASURED} - XANES_{FITTED})^2}{\sum XANES_{MEASURED}^2}, \quad (2.11)$$

where $XANES_{MEASURED}$ is XANES spectrum of unknown sample and $XANES_{FITTED}$ is XANES spectrum obtained from linear combination. The least value of R-factor is the best fitting to be accomplished.

2.5 Ca²⁺ hydration structure by QM/MM simulation

The structure of water molecule around essential ions, such as Ca²⁺, K⁺ and Cl⁻, including pure liquid water is widely controversial nowadays. Though the structure of ice or solid form of water has already cleared up as hexagonal crystalline structure for

ice usually found in the nature (ice 1h) (Lonsdale, 1958). Since the complexity the liquid system, there are many possible ways of making hydrogen bonds between water molecules. That makes it difficult to create the precise and accepted simulation. The simulation technique must be adapted and polished until reaching the acceptable goal. The Ca^{2+} hydration structure used in this thesis is originated from QM/MM simulation.

The Quantum mechanics/Molecular mechanics (QM/MM) simulation technique is a combination between of Quantum mechanics (QM) and Molecular mechanics (MM) simulations. QM is beneficial for more reliable interaction within the system, while MM is capable of modeling the large system quickly with minimized computation time. Thus, QM/MM allows for both save of computation time and efficiency of prediction. This technique can be done by considering different part with different approach or it can be clarified that the crucial part would be treated with QM, where that area is intensively concerned, and others would be considered with the classical interaction of MM, as shown in figure 2.22. Thus, one is able to appreciate more reliability of quantum mechanics while work loads are also reasonable with molecular mechanics.

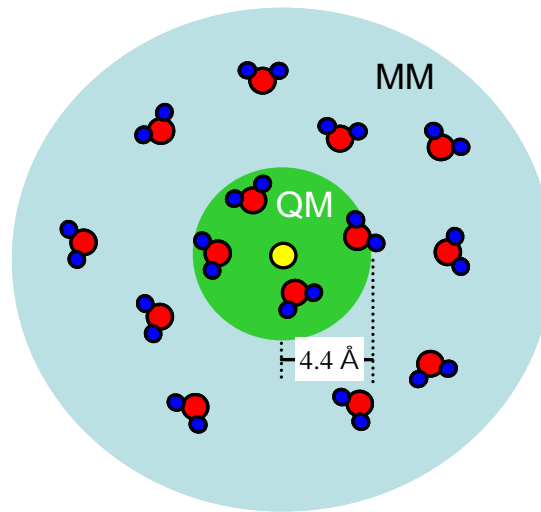


Figure 2.22 Schematic illustration of QM/MM modeling of QM and MM region.

Considering of both QM and MM employed in this technique, the suitable Hamiltonian to operate the system should be taken in account of quantum, mechanical frameworks and their intervention. The Hamiltonian for QM/MM can be expressed as

$$E_{total} = \langle \phi | H_{QM/QM} | \phi \rangle + \langle \phi | H_{MM/MM} | \phi \rangle + E_{MM/MM}, \quad (2.12)$$

where $\langle \phi | H_{QM/QM} | \phi \rangle$ accounts for the interaction energy of all particles in QM region, $E_{MM/MM}$ accounts for the interaction energy of all particles in MM region and $\langle \phi | H_{MM/MM} | \phi \rangle$ accounts of all interacting between particles in QM and MM region (Cramer, 2004).

For Ca^{2+} hydration QM/MM data used in this study, the 199 water molecules and Ca^{2+} ion were contained in a box with 18.17 Å length. The simulation was performed at 298 K with periodic boundary condition and the configurations of all elements in the system would be collected in every 0.2 fs after system's re-equilibration for 25000 time steps. Furthermore, to consider intensively in the area that should be the nearest

hydration shell, the QM region was 8.8 Å in diameter with Ca^{2+} located at center. The result of the simulation is shown as a snapshot of Ca^{2+} hydration structure shown in figure 2.23.

The distances of water molecules from Ca^{2+} ion are plotted within the duration of 50 ps as shown in figure 2.24. It can be seen that the first hydration shell is obviously seen around the distance of 2.4 Å. Nonetheless, some water molecules move in and out from the area of the nearest shell. In the simulation, the molecules that move from QM to MM region were treated with quantum mechanical and molecular mechanical forces and a smooth function in the transition area. The result of shell interchanging makes the value of coordination number changed with time between 6-8. In this thesis XANES will be used to evaluate the validation of coordination number obtained from this simulation.

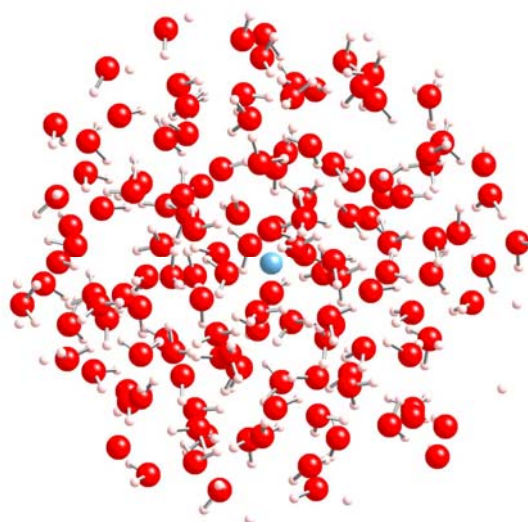


Figure 2.23 A snapshot of Ca^{2+} hydration structure by QM/MM simulation.

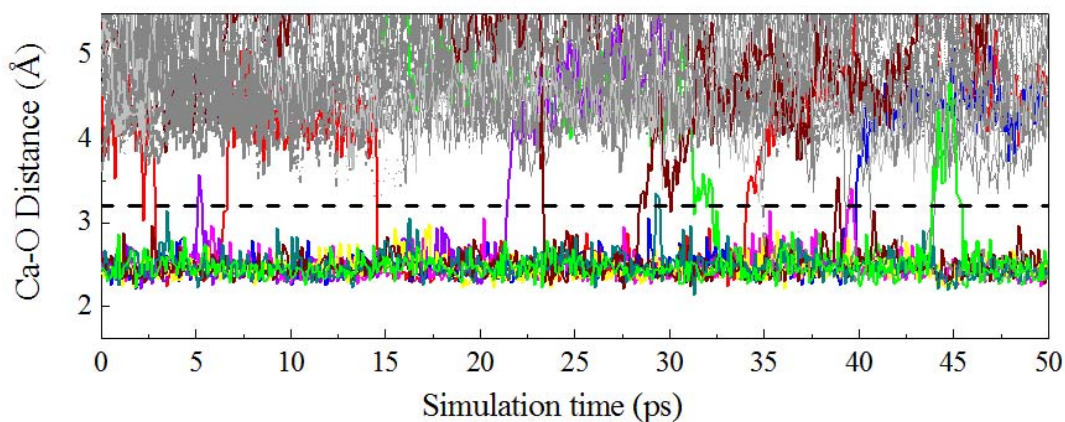


Figure 2.24 The trajectories of water molecules with respect to Ca^{2+} (Ca-O distances) from QM/MM calculation within 50 ps. The first hydration shell is clearly seen. Some molecules have entered or left the first shell in this simulation duration.

The distances of water molecules from Ca^{2+} ion are plotted within the duration of 50 ps as shown in figure 2.24. It can be seen that the first hydration shell is obviously seen around the distance of 2.4 Å. Nonetheless, some water molecules move in and out from the area of the nearest shell. In the simulation, the molecules that move from QM to MM region were treated with quantum mechanical and molecular mechanical forces and a smooth function in the transition area. The result of shell interchanging makes the value of coordination number changed with time between 6-8. In this thesis XANES will be used to evaluate the validation of coordination number obtained from this simulation.

2.6 Zinc oxynitride alloys

Zinc oxynitride alloys is speculated to be a composition of two parents elements, that is zinc oxide (ZnO) and zinc nitride (Zn_3N_2) with highly disordering degree, since the structure was not resolved by x-ray diffraction up to date. ZnO has wurtzite crystal structure and Zn_3N_2 has cubic anti-bixbyite form (Kuriyama, 1993). To generate “feff.inp” for XAS calculation by FEFF8.2, there are some parameters are needed for characterization. For wurtzite ZnO structure, the lattice parameters $a=0.3296$ and $c=0.5207$ nm (Wang, 2004) are used. For cubic anti-bixbyite structure Zn_3N_2 the parameter $a=0.9781$ nm (Kuriyama et al., 2007) is used in the calculation. The calculated XAS spectra are use in the LCA fittings.

To make candidate compound for zinc oxynitride alloys, some guess structure was created. One way is to replace some oxygen atoms in zinc oxide with nitrogen atoms to make $\text{ZnN}_x\text{O}_{1-x}$ crystal as shown in figure 2.25. It is speculated that the alloys may exist in this form in small area.

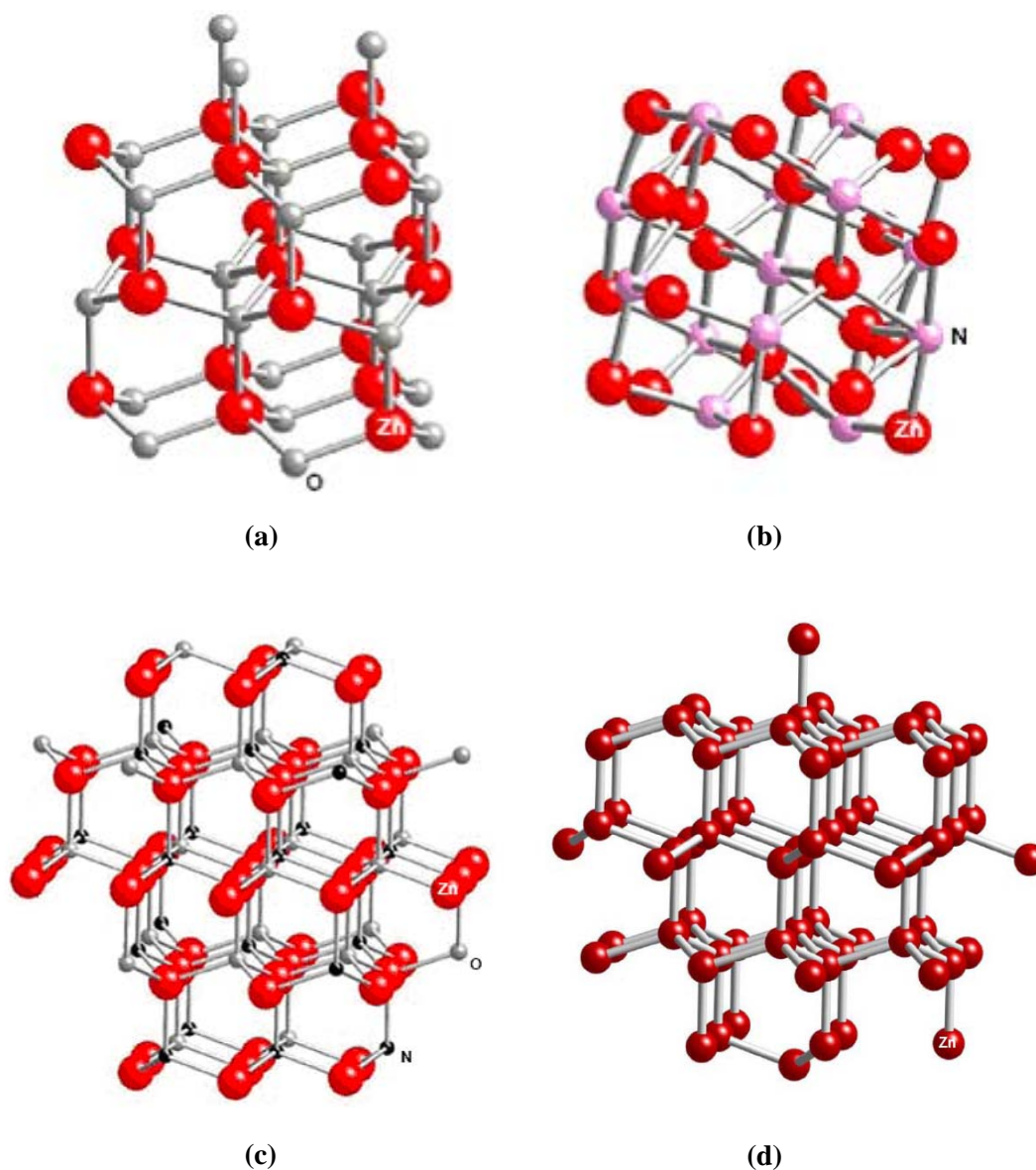


Figure 2.25 Ball-and-stick models for (a) zinc oxide (ZnO) and (b) zinc nitride (Zn₃N₂) and (c) ZnO_{0.5}N_{0.5} (d) Zn metal

On the other hand, for the case of unknown samples that are not totally zinc oxynitride, Zn K-edge XANES spectra of zinc oxynitride are considered as a combination of Zn metal and ZnO. The structure of Zn metal is hexagonal with lattice constant $a = 2.660 \text{ \AA}$, $c = 4.344 \text{ \AA}$ (Los Alamos National Laboratory, 2001) as also shown in figure 2.25.

In this thesis, three samples which are supposed to be zinc oxynitride alloys were prepared using rf sputtering under various conditions by Prof. Jiti Nukaew's research group at KMITL.

CHAPTER III

STRUCTURAL ANALYSIS FOR

Ca²⁺ HYDRATION STRUCTURE

In this chapter, the analysis of Ca²⁺ hydration structure by XAS is presented. First, the XAS measurement of Ca²⁺_{aq} is discussed. Then the data is analyzed in both EXAFS and XANES regions. The XAS spectra are simulated and compared with experiment. Finally, the Ca²⁺ hydration structure from candidate model is evaluated and the findings are discussed from the XAS point of view.

3.1 XAS measurement of Ca²⁺_{aq}

To prepare a sample for the XAS experiment, CaCl₂ was dissolved in de-ionized water to get the concentration of 2 m. Since the aqueous solution was under saturated then most of Ca components are present in the form of Ca²⁺ hydration structures in the solution, then Kimwipe® paper was used to absorb the aqueous solution and used in the transmission XAS experiment immediately.

The XAS measurement was performed in transmission mode using the facility at beamline 8 of the Siam photon Laboratory, SLRI, Nakhon Ratchasima. The Siam Photon Source was running at 1.2 GeV. The beam current was between 80-120 mA at the time of measurement. Si(111) double crystal monochromator was used in varying the photon energy. Ionization chambers were used in measuring of photon intensities. Kapton windows were used to isolate the ionization chambers from sample region

which was in ambient condition at atmospheric pressure. The length of the air gap was kept as small as possible to allow maximum photon flux through the sample.

The normalized K-edge XAS spectrum of $\text{Ca}^{2+}_{\text{aq}}$ of the absorption data is shown in figure 3.1. Resemble the $\text{Ca}^{2+}_{\text{aq}}$ XAS spectra reported in literatures, in the region below the 1s absorption edge, a small pre-edge peak around 4040 eV is observed. This feature has been identified as $1s \rightarrow 3d$ transition which is forbidden for octahedron symmetries (Fulton *et al*, 2003) This is a strong indication that the $\text{Ca}^{2+}_{\text{aq}}$ first hydration shell is noncentrosymmetric (D'Angelo *et al*, 2004). It is quite possible that the coordination number would differ from 8.

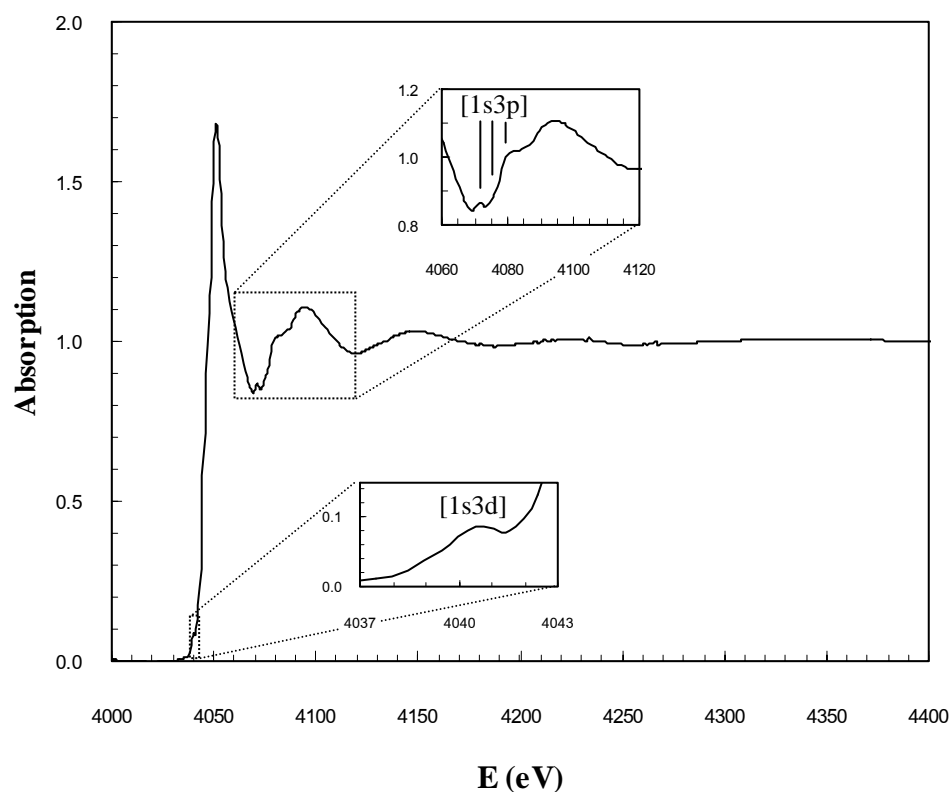


Figure 3.1 Normalized K-edge XAS spectrum of $\text{Ca}^{2+}_{\text{aq}}$. Shown in the lower and upper insets are [1s3d] and [1s3p] excitation channels.

In the region above the absorption edge, there exist several anomalous features as well. As shown in figure 3.1, a small peak and two humps between 4070-4080 eV were identified as [1s3p] transitions or KM_{23} edge (D'Angelo *et al*, 2004). Since the EXAFS oscillation in the low energy range of spectrum are distorted by these double electron excitation channels, this part of spectrum is not included in the EXAFS analysis in the following section.

3.2 Generation theoretical EXAFS spectra

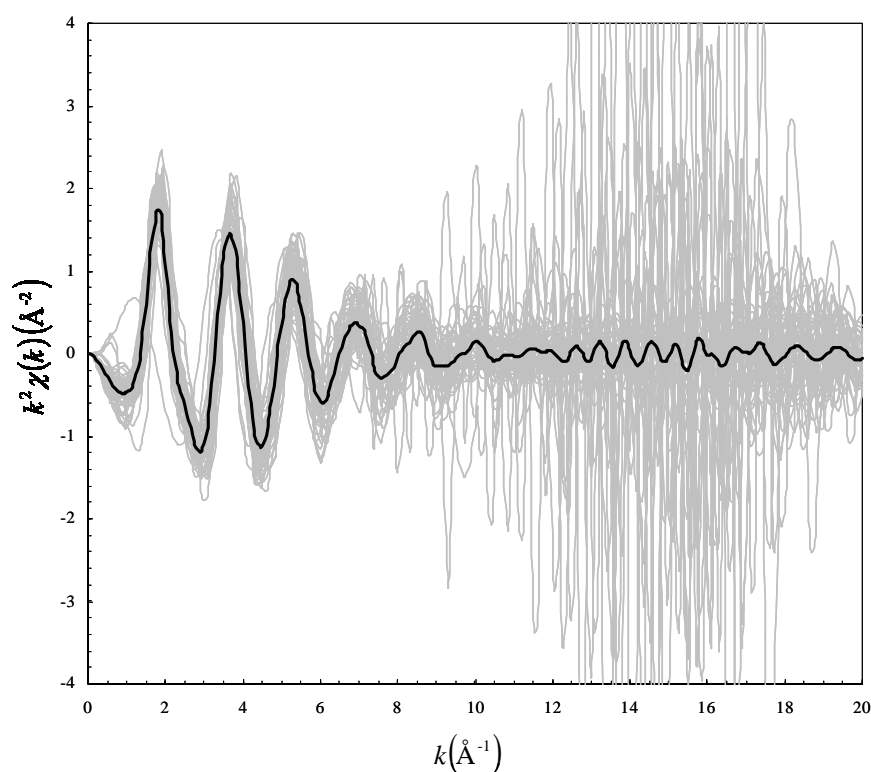


Figure 3.2 k^2 -weighted theoretical EXAFS spectra of Ca^{2+}_{aq} from 50 snapshots each separated by 0.5 ps time step. The average spectrum is shown in solid black line.

The data obtained from QM/MM simulation by Prof. Anan Tongraar was used for the generation of theoretical EXAFS spectra using FEFF8.2 program. The positions of calcium ion and oxygen atoms were used as scattering points in the calculation. Figure 3.2 shows the k^2 -weighted theoretical EXAFS spectra of $\text{Ca}^{2+}_{\text{aq}}$ from 50 snapshots each separated by 0.5 ps time step with the amplitude reduction factor (S_o^2) of 0.82 (Jalilehvand *et al.*, 2001).

It can be seen from the EXAFS spectra in figure 3.2 that there are very large variations between snapshots, especially for k higher than 8 \AA^{-1} . The theoretical EXAFS spectrum was obtained by averaging the spectra from every snapshot. This theoretical spectrum is used in the comparison with experimental EXAFS spectrum. It is noteworthy that the large variation of oscillations from each snapshot in the high k region was averaged out in the representative theoretical EXAFS spectrum as shown in figure 3.2. Therefore, the comparison would be focused on oscillations in the region of k value below 8 \AA^{-1} . The structural parameters extracted from theoretical model used in this work such as R_0 (nearest neighbor hydration shell distance), σ^2 (Debye-Waller factor) and N (coordination number) are obtained from fitting of radial distribution function (RDF) with Gaussian distribution function as shown in figure 3.3 and can be summarized in table 3.1 along with the values published in literatures. It could be seen that, even though there is good agreement in R_0 value, the theoretical simulations give quite large variation of σ^2 and N values. Therefore, the experiment verification is needed crucially.

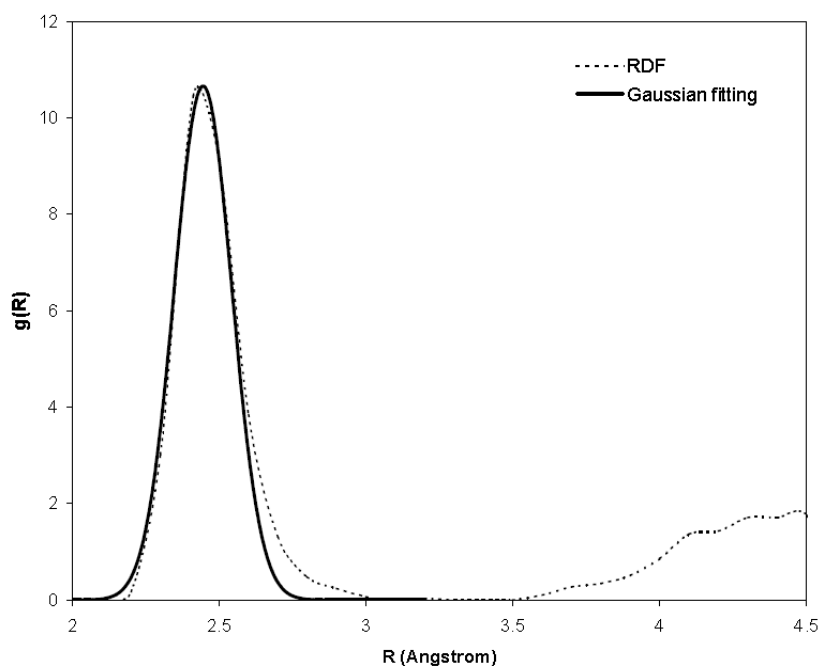


Figure 3.3 Fitting of radial distribution function (dashed line) with Gaussian distribution function (solid line).

Table 3.1 Results from theoretical simulations for $\text{Ca}^{2+}_{\text{aq}}$ structural parameters: R_0 is nearest neighbor hydration shell distance, N is coordination number and σ^2 is Debye-Waller factor.

	R_0 (Å)	σ^2 (Å ²)	N
Jalilehvand <i>et al.</i> , 2001(MD)	2.40	0.020	8.0
D'Angelo <i>et al.</i> , 2004 (MD)	2.48	0.008	7.9
Dang <i>et al.</i> , 2006 (MD)	2.45	0.0066	6.5
Tongraar, (QM/MM)	2.42	-	7.4 ± 0.1
	2.45^a	0.0096^a	6.8^a

^aFitted parameters from RDF with Gaussian distribution function

3.3 EXAFS Analysis

The experimental absorption data was analyzed using *ATHENA* software to get the EXAFS spectra. The curve fitting was done for the k^2 -weighted spectrum over the k -range of 3.5-8.0 Å⁻¹ using a window of Hanning type. From direct EXAFS fitting of Ca-O bond, the structural parameters can be obtained. Shown in figure 3.4 are three k^2 -weighted K-edge EXAFS spectra: the experimental spectrum, the theoretical spectrum, and the spectrum from direct fitting. In general, it may be seen that the three spectra are in good agreement over the region 3.5-8.0 Å⁻¹. Therefore, the QM/MM simulation appears to give a good overview of the hydration structure, qualitatively and the reliable structural parameters would be obtained from fitting.

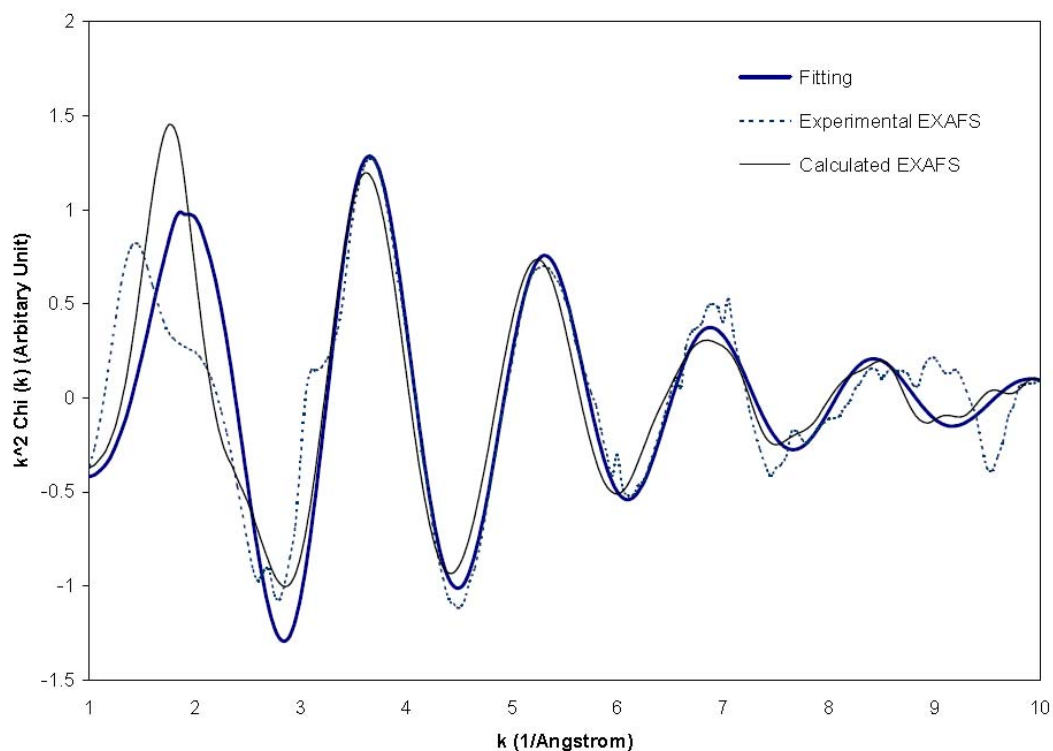


Figure 3.4 Comparison of k^2 -weighted EXAFS spectra of $\text{Ca}^{2+}_{\text{aq}}$: theoretical QM/MM spectrum, measurement spectrum, and fitting.

From curve fitting of experimental data to the EXAFS equation using *IFEFFIT*, important structural parameters were extracted. The corresponding Fourier transform of the three spectra are shown in real space in figure 3.5. It can be seen that the theoretical spectra can reproduce the experimental data nicely. Indeed, all three spectra show quite good agreement. The first peak position in real space EXAFS can be converted into the radius of first hydration shell.

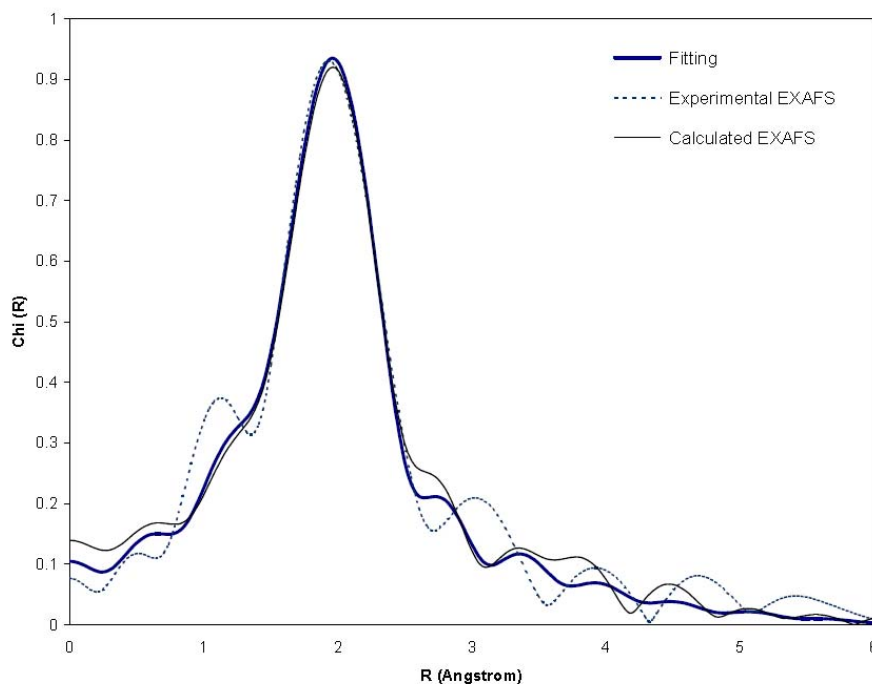


Figure 3.5 Comparison of Fourier transforms of EXAFS spectra of $\text{Ca}^{2+}_{\text{aq}}$: theoretical QM/MM spectrum, measurement spectrum, and fitting.

In this work, the best fitting parameters obtained from this work for average Ca-O distance (R_0), Debye-Waller factor (σ^2) and coordination number (N) are 2.431 ± 0.011 , 0.009 and 6.56 ± 0.316 respectively, which are the results from the least R-factor as shown in table 3.2 and summarized together with the experimental values published in the literature in table 3.3.. However, the parameters from fitting seem not to be in good agreement with the structural parameters, which directly extracted from the simulations shown in table 3.1, especially for N where it is 7.4 ± 0.1 from the simulation compared with 6.56 ± 0.316 from the fitting. It is quite a large difference. This difference can be explained this result with the parameter obtained directly from fitting with calculated spectrum as shown in figure 3.6 and resulted in table 3.4. The comparison shows that the calculated EXAFS shows the accuracy of QM/MM

simulations evidenced by the agreement of simulated and calculated EXAFS in both k and R space, but not for actual structural parameters. Results from fitting are similar to the parameters from RDF fitting shown in table 3.1. Thus, EXAFS analysis can tell the accuracy of models, but the structural parameters can be obtained directly from the simulation and XANES analysis may be another chance to verify the existence of the structures.

Table 3.2 Fitting for $\text{Ca}^{2+}_{\text{aq}}$ structural parameters of measured EXAFS: R_0 is nearest neighbor hydration shell distance, N is coordination number and σ^2 is Debye-Waller factor.

R_0 (Å)	N	S_0^2	σ^2 (Å ²)	R -factor
2.433 ± 0.0130	7.56 ± 0.619	0.83	0.010	0.0015
2.433 ± 0.0130	7.65 ± 0.626	0.82	0.010	0.0015
2.433 ± 0.0130	7.74 ± 0.634	0.81	0.010	0.0015
2.433 ± 0.0136	8.03 ± 0.793	0.82	0.013	0.0046
2.433 ± 0.0130	7.65 ± 0.626	0.82	0.012	0.0032
2.432 ± 0.0124	7.28 ± 0.484	0.82	0.011	0.0022
2.432 ± 0.0119	6.91 ± 0.375	0.82	0.010	0.0015
2.432 ± 0.0113	6.56 ± 0.316	0.82	0.009	0.0012
2.431 ± 0.0108	6.21 ± 0.317	0.82	0.008	0.0013

Table 3.3 Results from the EXAFS fitting for $\text{Ca}^{2+}_{\text{aq}}$ structural parameters: R_0 is nearest neighbor hydration shell distance, N is coordination number and σ^2 is Debye-Waller factor. R-factor is defined by equation (2.11)

	R_0 (\AA)	σ^2 (\AA^2)	N	R -factor
Jalilehvand <i>et al.</i> , 2001	2.461 ± 0.009	0.011	8	
Fulton <i>et al.</i> , 2003	2.437 ± 0.010	0.012	7.2 ± 1.2	0.01
D'Angelo <i>et al.</i> , 2004	2.49 ± 0.01	0.016	8.1	
Dang <i>et al.</i> , 2006	2.429 ± 0.030	0.0115	6.8 ± 1.0	
This work	2.431 ± 0.011	0.009	6.56 ± 0.316	0.001

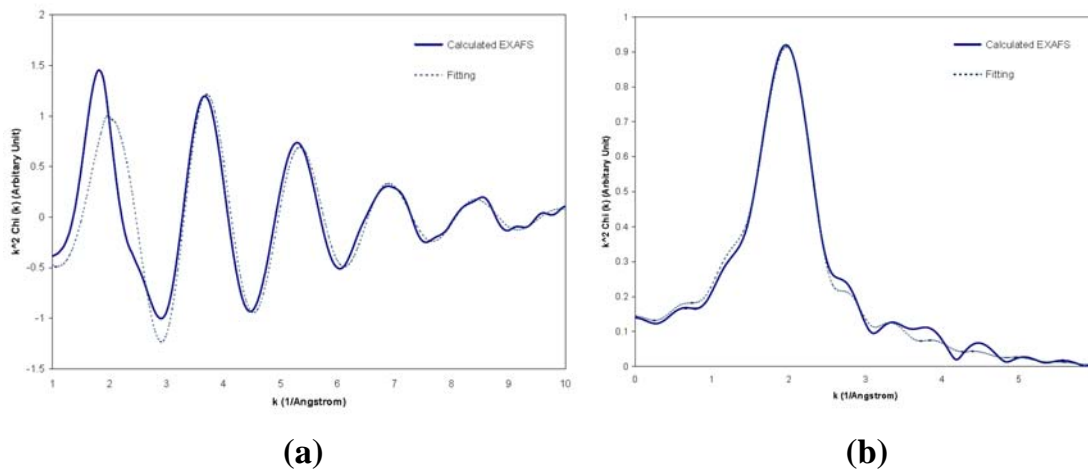


Figure 3.6 Comparison of (a) k-space and (b) real space EXAFS spectra of $\text{Ca}^{2+}_{\text{aq}}$: theoretical QM/MM spectrum (Solid line) and its fitting (dashed line).

Table 3.4 Fitting for $\text{Ca}^{2+}_{\text{aq}}$ structural parameters of calculated EXAFS: R_0 is nearest neighbor hydration shell distance, N is coordination number and σ^2 is Debye-Waller factor.

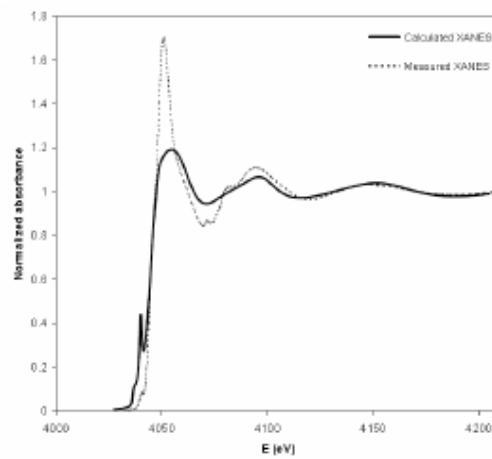
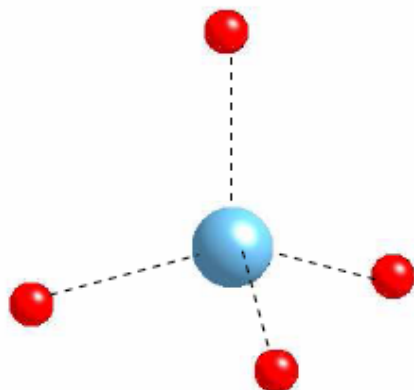
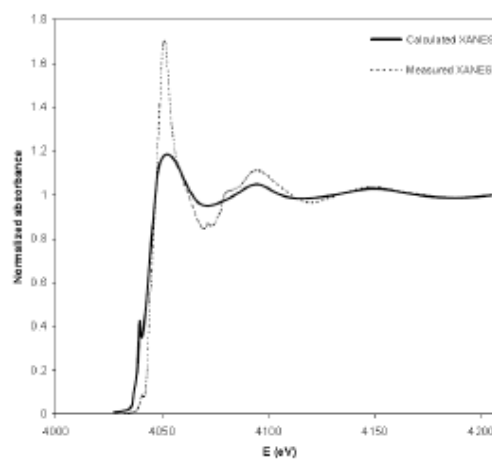
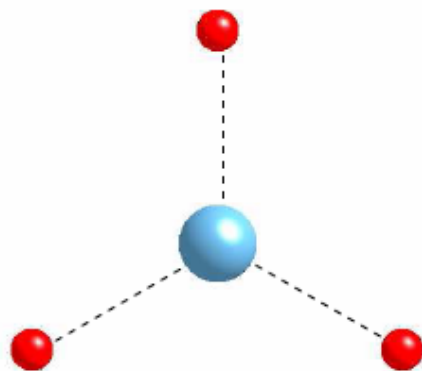
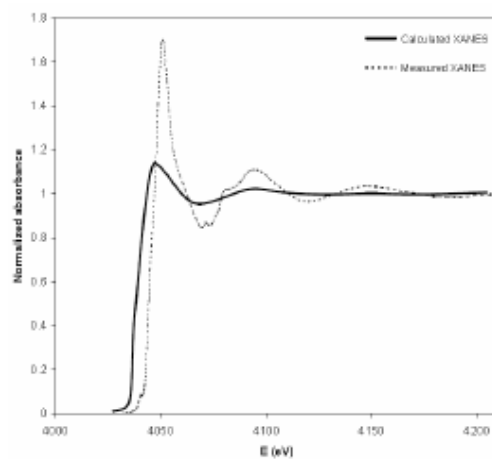
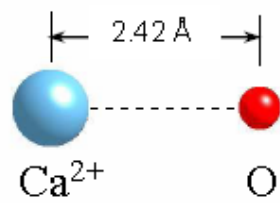
R_0 (Å)	N	S_0^2	σ^2 (Å ²)	R -factor
2.445 ± 0.0249	6.81 ± 0.223	0.84	0.012	0.0014
2.445 ± 0.0249	6.89 ± 0.226	0.83	0.012	0.0014
2.445 ± 0.0249	6.97 ± 0.229	0.82	0.012	0.0014
2.445 ± 0.0249	6.67 ± 0.146	0.82	0.011	0.0006
2.445 ± 0.0249	6.37 ± 0.100	0.82	0.010	0.0003
2.445 ± 0.0249	6.09 ± 0.123	0.82	0.009	0.0006
2.445 ± 0.0249	5.81 ± 0.184	0.82	0.008	0.0014

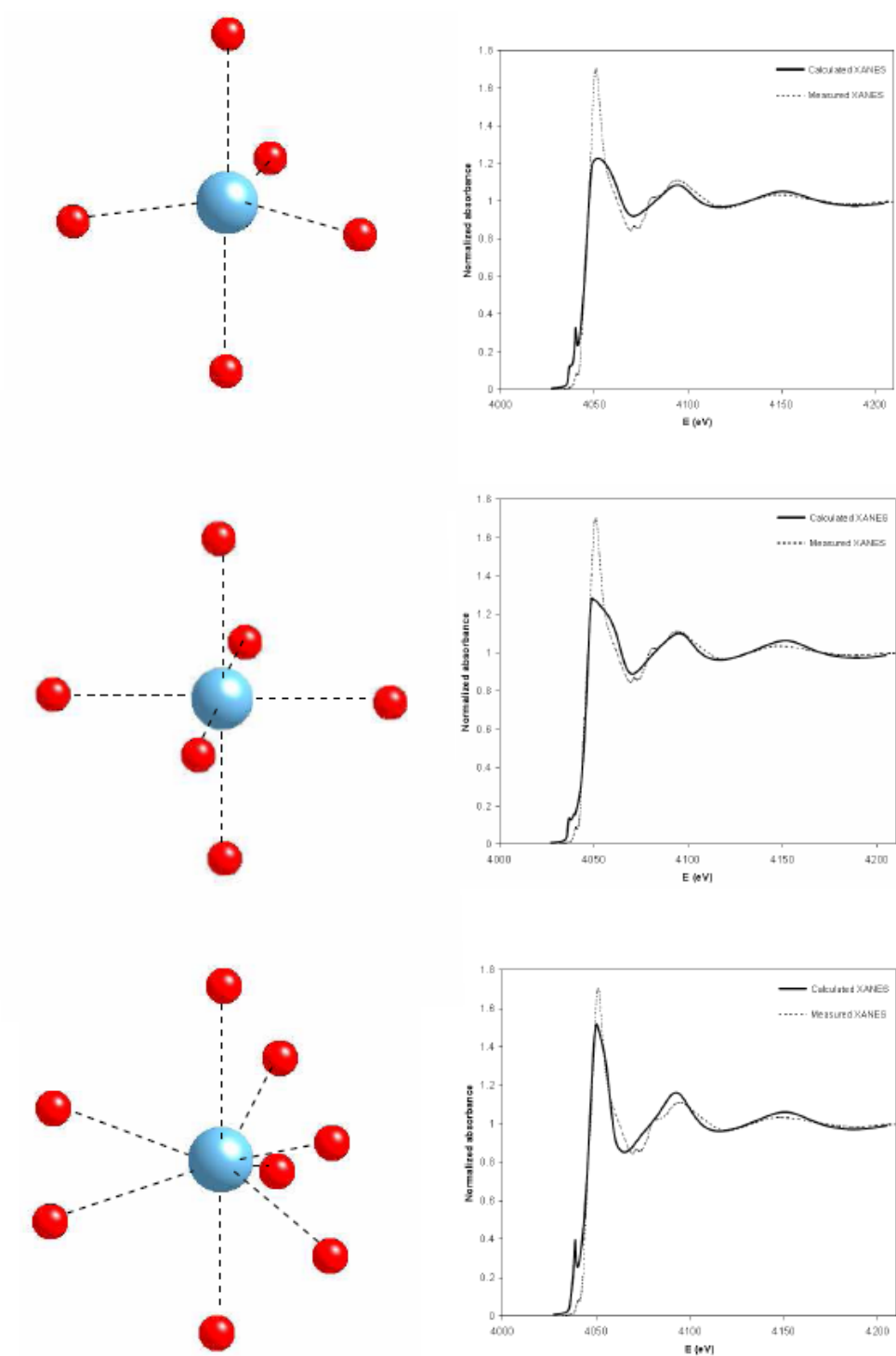
3.4 XANES Analysis

The experimental $\text{Ca}^{2+}_{\text{aq}}$ XANES spectra have been reported by several groups, however, the XANES simulation was left out. Indeed, up to present, there is no report on the $\text{Ca}^{2+}_{\text{aq}}$ theoretical XANES spectrum. In this section, it is shown that XANES can provide the complementary information on local structure verification.

It is generally accepted that XANES is sensitive to the local structure around the absorbing central atom. Therefore, the reliable theoretical model should give compatible theoretical XANES spectrum compared with the experimental spectrum.

Firstly, the trial simulated Ca-O structures were used to calculate XANES spectra to investigate the spectrum change affected from different coordination number as shown in figure 3.7. It can be seen that the features of 6 and 8 oxygen atom XANES are quite similar to the experimental one.





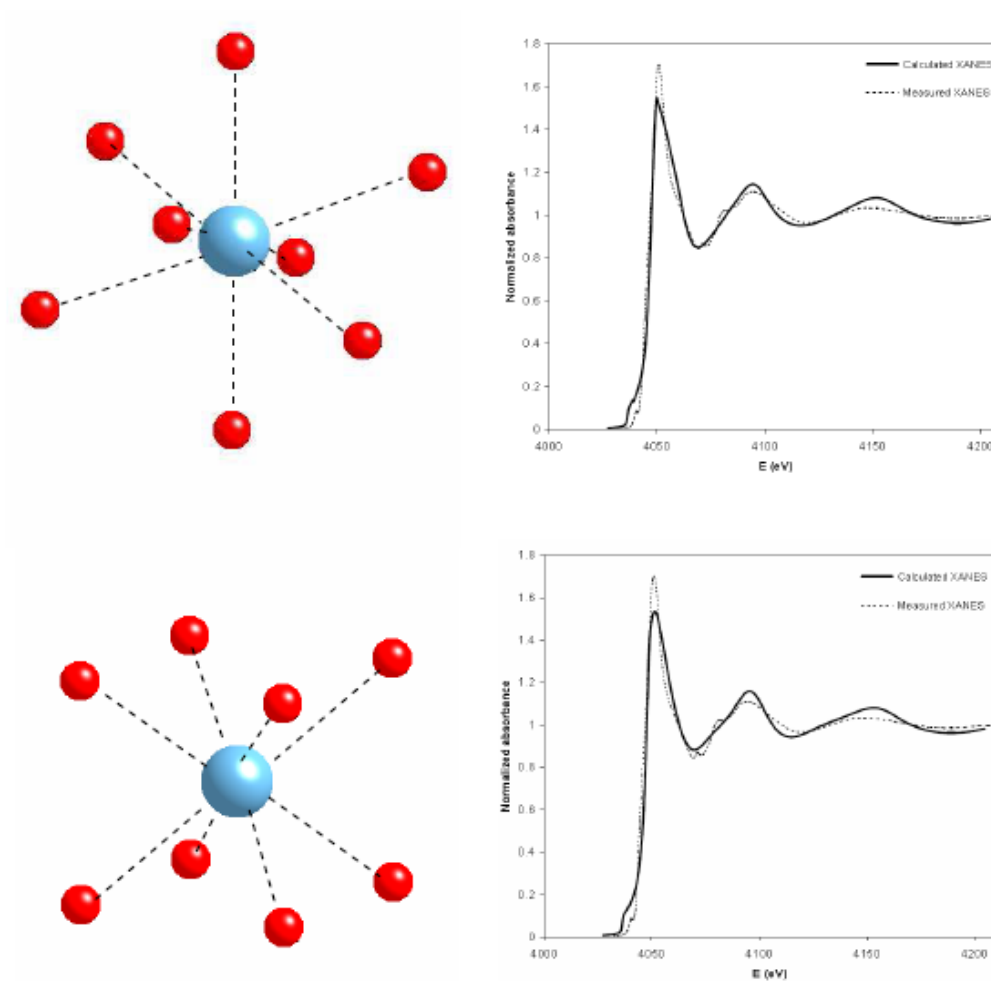


Figure 3.7 Calculated K-edge XANES spectra of $\text{Ca}^{2+}_{\text{aq}}$ hydration structure from defined Ca and O structures compared with the dashed line from measurement.

After that, in a similar way as described in the above section, the data obtained from QM/MM simulation was used for the generation of theoretical XANES spectra using FEFF8.2 code. The positions of calcium ion and oxygen atoms were used as scattering points in the calculation using the procedure described in chapter II. Figure 3.8 shows the theoretical XANES spectra of $\text{Ca}^{2+}_{\text{aq}}$ from 50 snapshots each separated by 0.5 ps time step.

Since the water molecules do not form stable geometric structure around Ca^{2+} ion, it can be expected that the local structure changes for every time step. This is revealed in the XANES spectra simulation shown in figure 3.8. There are variations among the calculated spectrum from each time step. However, even the dynamic XANES spectrum changing with time, the average XANES spectrum has a well defined shape resemble that of the experimental spectra. This average XANES spectra is used as the representative theoretical QMM/MM XANES spectra for further comparison.

To examine closely, the correlation of local structure to the XANES spectrum, four snapshots at time 5, 10, 15, and 20 ps has been selected and shown in figure 3.9.

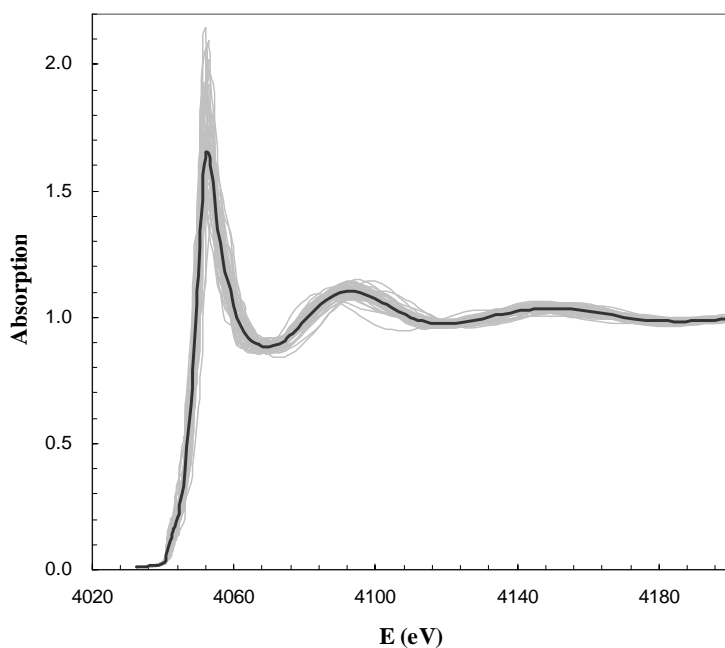


Figure 3.8 Calculated K-edge XANES spectra of $\text{Ca}^{2+}_{\text{aq}}$ hydration structure from 50 QM/MM snapshots with 0.5 ps time step, all shown in gray line. The average spectrum is shown in black line.

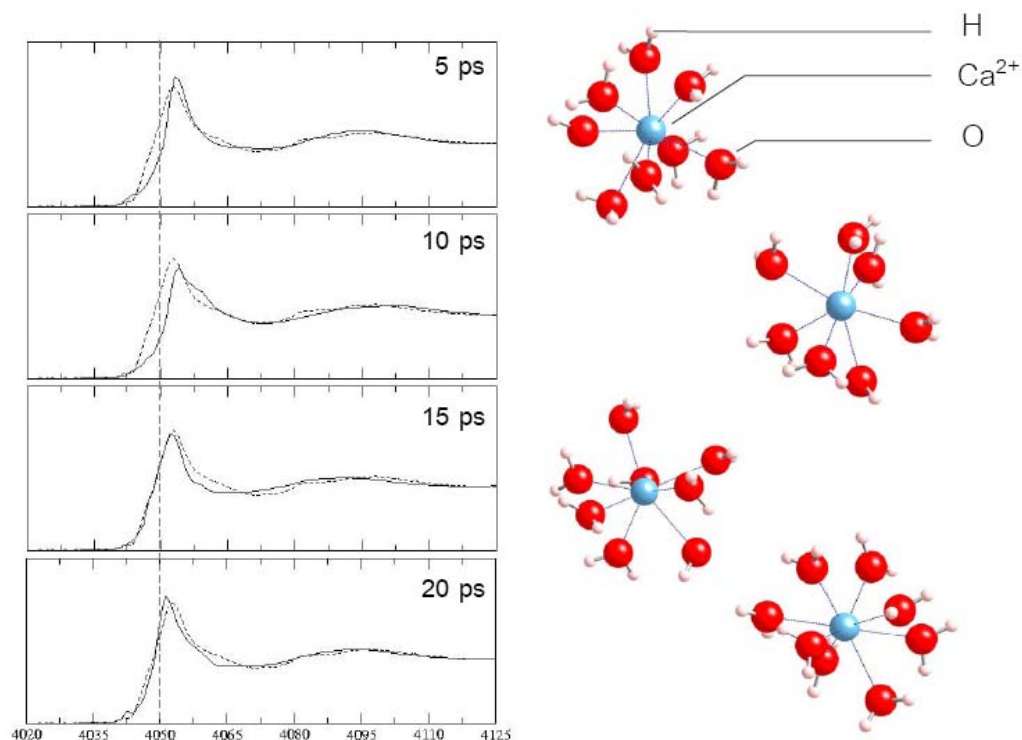


Figure 3.9 K-edge XANES spectra of $\text{Ca}^{2+}_{\text{aq}}$ from four QM/MM snapshots (solid line) compared with experimental data (dashed line). The insets are correspondent Ca^{2+} hydration structure models within the first shell.

It can be seen that, the theoretical XANES from each snapshot displays some variation when compared with the experimental data. There are over-shooting and under shooting areas among the selected spectra. The frames at 5, 15 and 20 ps, have the same coordination number which is $N=8$, while the frame at 10 ps have $N=7$. Roughly, the frame with $N=8$ tend to produce XANES spectrum with sharp white line and absorption edge shift to lower energy. The frame with $N=7$ tend to give XANES spectrum with broad white line and absorption edge shift to higher energy. The post

edge hump area seem to be over shooting for $N = 7$. These observations may be used as guidelines to judge the resemblance of theoretical and experimental XANES spectra qualitatively. The comparison between the two spectra is shown in figure 3.10.

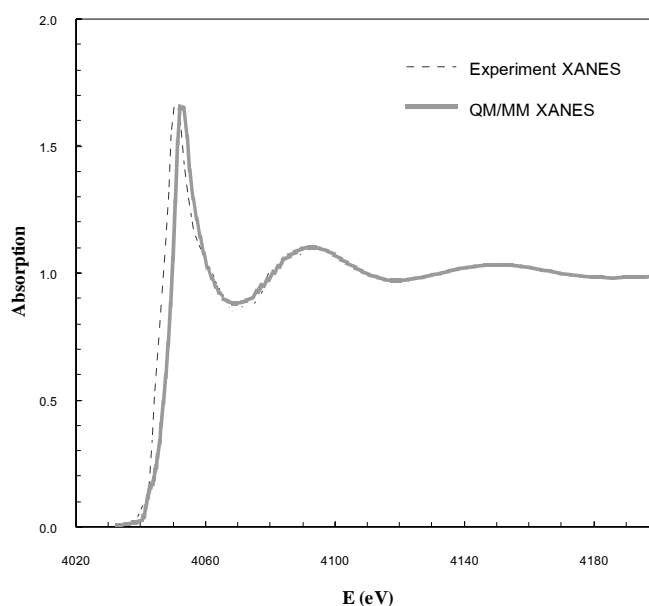


Figure 3.10 Comparison between experimental (dashed) and theoretical QM/MM (hatched) K-edge XANES spectra of $\text{Ca}^{2+}_{\text{aq}}$.

Qualitatively, it can be concluded that the theoretical QM/MM XANES spectrum can reproduce the features presented in experimental XANES spectrum very well. With the omission of [1s3p] channels, the [1s3d] multi electron excitations pre-edge feature could also be reproduced by the simulations. This pre-edge peak is the supporting evidence for the noncentrosymmetric structure of the first hydration shell described hitherto. The absorption edge energy of the theoretical spectrum is about 3 eV higher than that of the experimental one, which is quite normal for FEFF calculation. Quantitatively, for energy higher than 25 eV above the edge, into the

EXAFS region, the two spectra can be fitted perfectly, thus the average picture seems to be reasonable. Therefore, the reliability of QM/MM hydration structure model (dynamic) used in this work is very well supported by the XANES measurement (static).

CHAPTER IV

STRUCTURAL ANALYSIS

OF ZINC OXYNITRIDE ALLOYS

In this chapter, the structural analysis of zinc oxynitride alloys based on XAS measurement is discussed.

The zinc oxynitride samples used in this study were obtained from Prof. Jiti Nukaew's research group at Nanotechnology Research Centre, King Mongkut's Institute of Technology Ladkrabang (KMITL). Three zinc oxynitride thin film samples were deposited on silicon substrate using reactive gas-timing RF-sputtering method. Zn metal, oxygen (O₂) and nitrogen (N₂) gases are the starting material. The gas timing sequence between O₂ and N₂ was selected to ensure the uniformity throughout the film. By changing the O₂/N₂ gas timing, it was found that the composition of O₂ and N₂ in the alloys could be varied. By varying the O₂/N₂ compositions it was expected that the electrical and optical properties of the alloys can be altered and used for new applications. The three samples used in this study were synthesized under O₂/N₂ gas timing different conditions. The thicknesses of the films were about 2-3 μm.

Because the disordering structure of zinc oxynitride alloys, the samples can not be characterized by x-ray diffraction. Therefore, XAS is the only mean available for the atomic structural investigation.

The XAS measurement was done in fluorescence mode, using the XAS beamline of the Siam Photon Laboratory, Synchrotron Light Research Institute. Si(111) double

crystal monochromator was used for photon energy selection. Multi-element high purity germanium detector was used to detect the fluorescence x-ray. The sample was at atmospheric pressure and ambient condition during the measurement. The Siam Photon source was running at 1.2 GeV electron beam energy with the current between 80-100 mA.

Due to the limitation in XAS measurement in soft x-ray region, there was no measurement on O and N absorption edge. Therefore, in this study we focused on the XANES measurement of Zn K-edge. The measured XANES spectra of 3 samples are normalized and shown in figure 4.1.

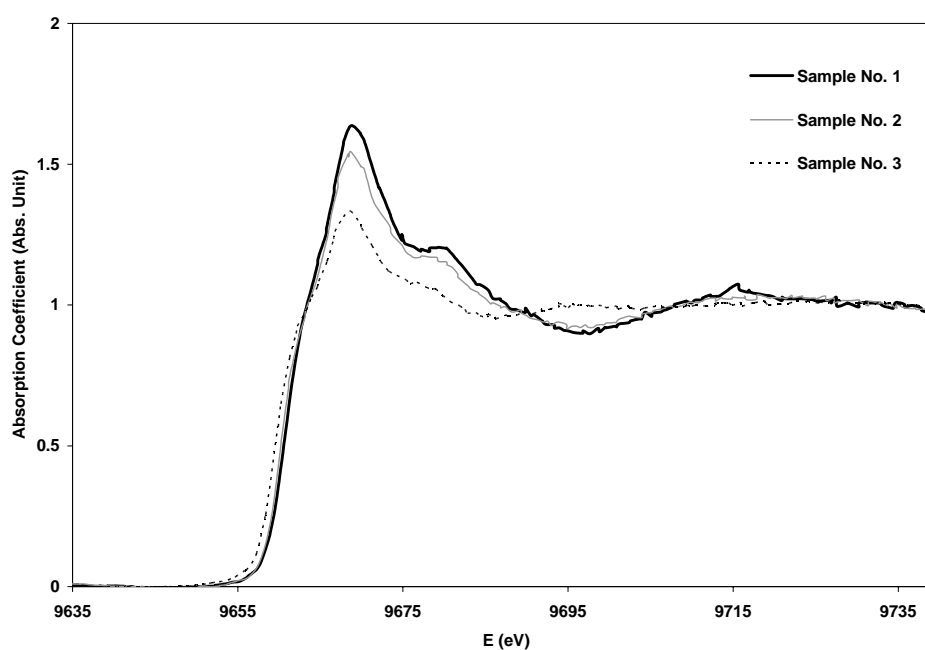


Figure 4.1 Zn K-edge XANES normalized spectra of three zinc oxynitride samples

The measured Zn K-edge XANES spectra of zinc oxynitride alloys do not match any known reference compound available in the datum base. To make it worse, there is no possibility to get supporting information from x-ray diffraction. Therefore, the theoretical XANES from candidate compounds must be generated and compared with the experiment.

A variety of candidate compounds were considered in the making of the theoretical XANES spectra database. First, the true fictitious alloys, $\text{ZnO}_{1-x}\text{N}_x$ such as the one shown in figure 2.25 were considered. The candidate models were created by using ZnO wurtzite framework and replace some oxygen atoms with nitrogen to get the desired compositions. Clearly, from electron counting, this fictitious alloys is not exist in the large crystal form due to insufficient electron to form tetrahedral bonding network. However, it may be possible that the alloys can exist in nanocrystal form such as the case of indium oxynitride.

The second type of candidate compounds was created by considering phase separation possibility. If the sample consists of ZnO and Zn_3N_2 domains separately, based on LCA, the data could be generated by using the linear combination between XANES spectra of zinc oxide and zinc nitride with various compositions.

After the theoretical XANES database has been compiled, the spectra can be used to compared and fitted with the experiment spectra.

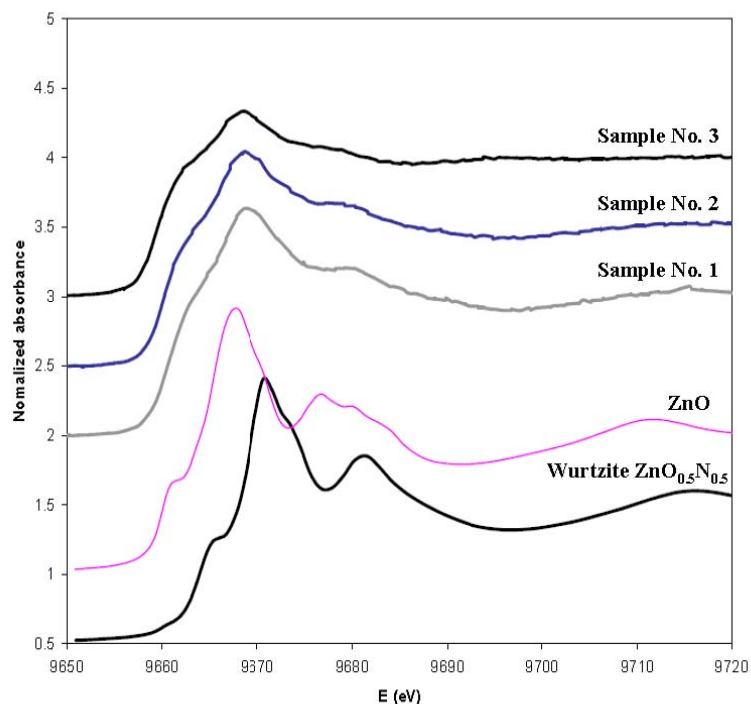


Figure 4.2 Comparison of the measured Zn K-edge XANES spectra of zinc oxynitride, and simulated spectrum from ZnO and ZnO_{0.5}N_{0.5} alloys.

In the first approach, the simulated XANES spectrum from the true fictitious ZnO_{1-x}N_x alloy does not seem to be a good fit. As shown in figure 4.2, the absorption edge is shifted away toward the high energy for more than 10 eV for ZnO_{0.5}N_{0.5} fictitious alloys. The overall feature of simulated spectra looks like that of ZnO with energy shift. The blue shift in absorption edge is due to the higher oxidation state of Zn. However, the features in experimental spectra do not match with the simulated spectra. Therefore, this approach was abandoned eventually.

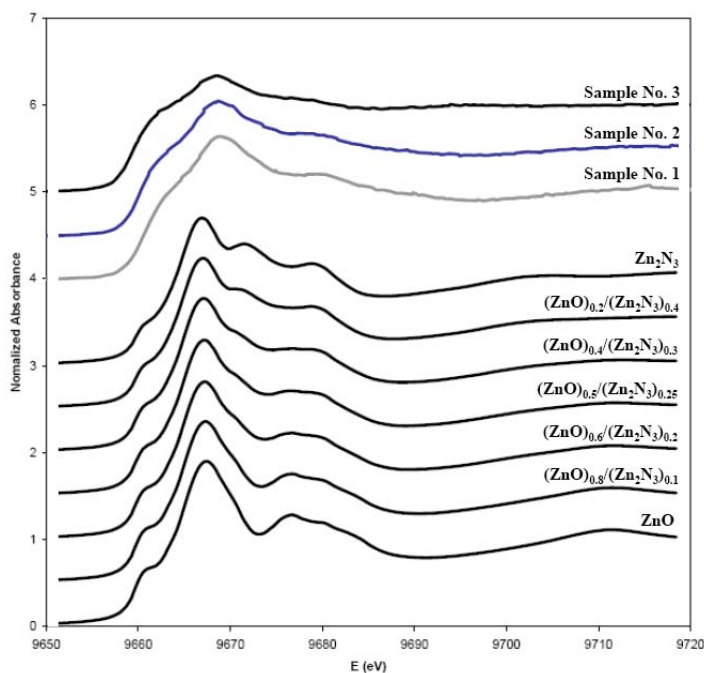


Figure 4.3 Comparison of the measured Zn K-edge XANES spectra of zinc oxynitride and simulated spectra from linear combination of ZnO and Zn_3N_2 with various proportions.

In the second approach, using some trial proportions of ZnO and Zn_3N_2 to get Zn K-edge XANES linear combination, mixed XANES spectra can not reproduce the measured XANES spectra as shown in figure 4.3. Therefore, we concluded that the structure of unknown samples may not be explained by phase separation of ZnO and Zn_3N_2 .

Still base on the idea of LCA, the other possible combinations are further considered. It was found that the combination between ZnO and Zn metal may give all features observed in the experiment as shown in figure 4.4.

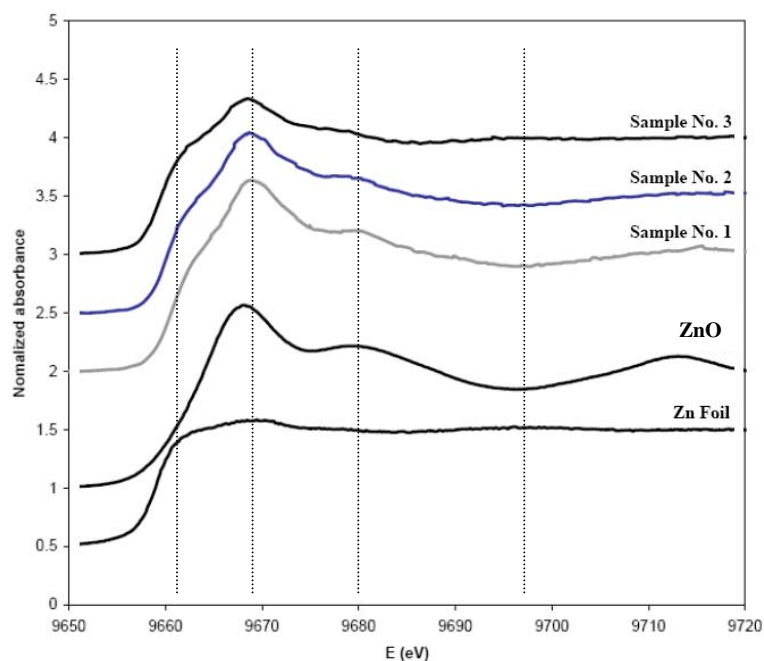


Figure 4.4 Comparison of the measured Zn K-edge XANES spectra of zinc oxynitride and the reference spectra of ZnO and Zn metal.

By considering ZnO and Zn metal as parent components, the XANES spectra of unknown samples are fitted with XANES of parent components with varying proportion using LCA method. The fitting was performed in *ATHENA* with linear combination analysis tool. The results for fitted XANES spectra are compared with the measured XANES spectra, as shown in figure 4.5. In addition, the proportions of two parent components obtained from the fitting are shown in Table 4.1.

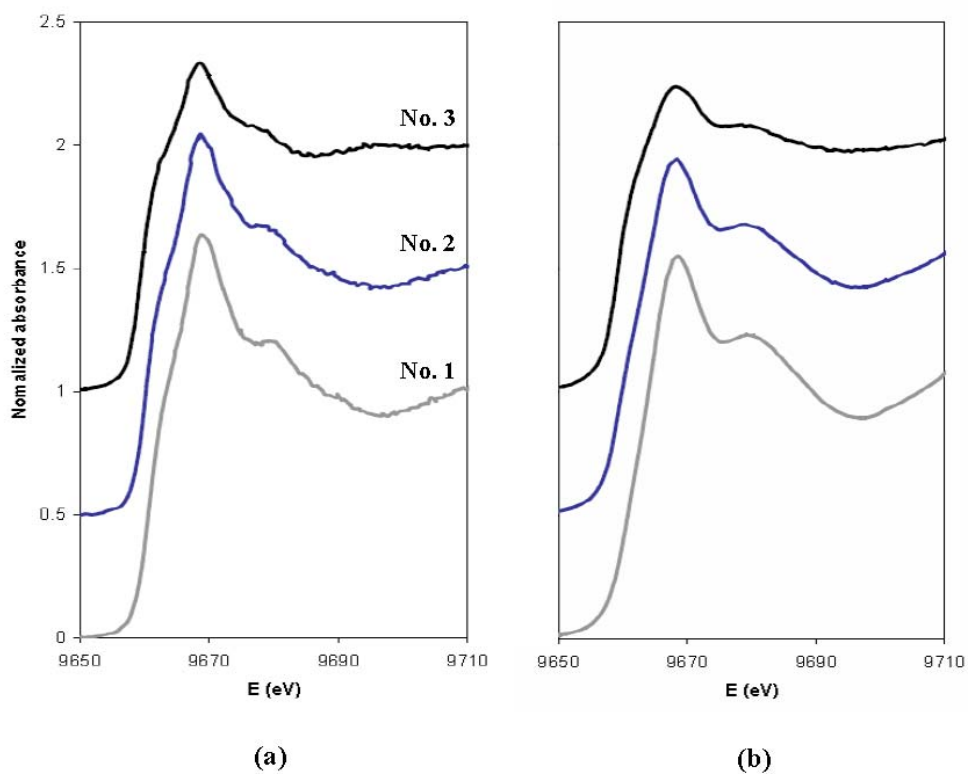


Figure 4.5 K-edge XANES of zinc oxynitride samples (a) and their fitting (b).

Table 4.1 Proportion of ZnO and Zn metal, and R-factor of three unknown samples obtained from linear combination analysis

<i>Sample</i>	<i>Proportion of ZnO</i>	<i>Proportion of Zn metal</i>	<i>R-factor</i>
No. 1	0.820	0.180	0.001851
No. 2	0.630	0.370	0.002050
No. 3	0.283	0.717	0.001269

It can be seen that, the simulated LCA XANES spectra can fit nicely to the experiment spectra. The low value of R-factor obtained from the fit ensures that the fit is reliable. Therefore, from the XAS point of view, it may be concluded that the zinc oxynitride films used in this work are mainly composed of ZnO and Zn metal in phase separated domains. It may be speculated that the Zn metal nanocrystal domains may be formed between ZnO nanocrystal domains when the growth is in Zn-rich condition. Since, those nanocrystal domains are very small they can not be resolved by normal x-ray diffraction measurement. With the presence of oxygen, nitrogen may prefer to form NO_x species more than bonding with Zn. The NO_x can be absorbed and trapped between the nanocrystal domain boundaries and no zinc oxynitride alloys was formed. Therefore, the question on the atomic scale structure of zinc oxynitride remains to be unsolved until the real alloys can be made available in the future.

CHAPTER V

CONCLUSIONS

In this thesis, two disorder systems, Ca^{2+} hydration structure and zinc oxynitride alloys, were studied by XAS. Because the atomic scale structure of the two systems can not be electively solved by standard techniques such as x-ray diffraction or high resolution electron microscope due to lacking of long range ordering.

Dynamic Ca^{2+} hydration structures simulated by QM/MM MD were used as the model structure to generate theoretical K-edge XAS spectra, both XANES and EXAFS region for comparison with the experiment. The XAS data taken at the Siam Photon Laboratory, show similar features to the spectrum published in the literature. The theoretical EXAFS spectrum can well reproduce the experimental EXAFS spectrum. From the fitting of EXAFS spectra the structural parameters were obtained. The Ca-O distance of $2.431 \pm 0.011 \text{ \AA}$, the coordinate number of 6.56 ± 0.316 and the Debye-Waller factor of 0.009 \AA^2 were obtained from curve fitting. These were well compared with the parameters suggested by RDF fitting of theoretical QM/MM simulation of 2.445 \AA , 6.8, and 0.0096 \AA^2 respectively.

The other alternative way to characterize the disorder system is the direct investigation of compatibility between the structural simulations for the nearest neighbor distance and the correspondent XANES spectra. In this case the theoretical XANES of $\text{Ca}^{2+}_{\text{aq}}$ was in very good agreement with the experimental spectrum. These results confirm the validity of the Ca^{2+} hydration structure obtained from QM/MM MD simulation by Assoc. Prof. Anan Tongraar.

In the second part of this thesis work, zinc oxynitride thin films prepared by Prof. Jiti Nukaew and his colleagues were characterized by XANES. Based on linear combination of reference parent components, a database for XANES spectra has been generated. The XANES analysis showed that the three samples may not mainly be the combination of ZnO and Zn₃N₂ as first expected, but mostly the combination of ZnO and Zn metal possibly co-exists in the form of nanocrystal domains. Although the XANES analysis shows that the samples are not mainly composed of ZnO and Zn₃N₂, because the simulated spectra of ZnO_{0.5}N_{0.5} is similar to that of ZnO, some of alloys can be ZnO_{0.5}N_{0.5}. That may be interesting for future study.

Thus, in this thesis, the XAS studies of disorder material structures have been performed. As summarized in figure 5.1, the candidate model or simulated structure of disordered system is used to calculate the theoretical XANES and EXAFS spectra, by FEFF8.2 code. The spectrum generation is the most important step especially when the structure is unknown or there is some dynamic change. Then, the theoretical spectrum can be compared with the actual measured spectrum with the analysis package. In *ATHENA*, the XAS spectrum is normalized. After normalization XANES spectrum is ready to be compared. On the other hand, EXAFS spectrum has to be converted to k-space and Fourier transformed to R-space before comparing with the experimental result and further EXAFS fitting in *ATHEMIS*. After fitting, the important structural parameters are obtained. The residue or R-factor can be used as the guideline whether the fit is reliable or not. Low value of R-factor would be good indication of the compatibility between theory and experiment. It is suggested that, this procedure can be used as the alternative way for atomic scale structural characterization when standard methods do not give any satisfactory result.

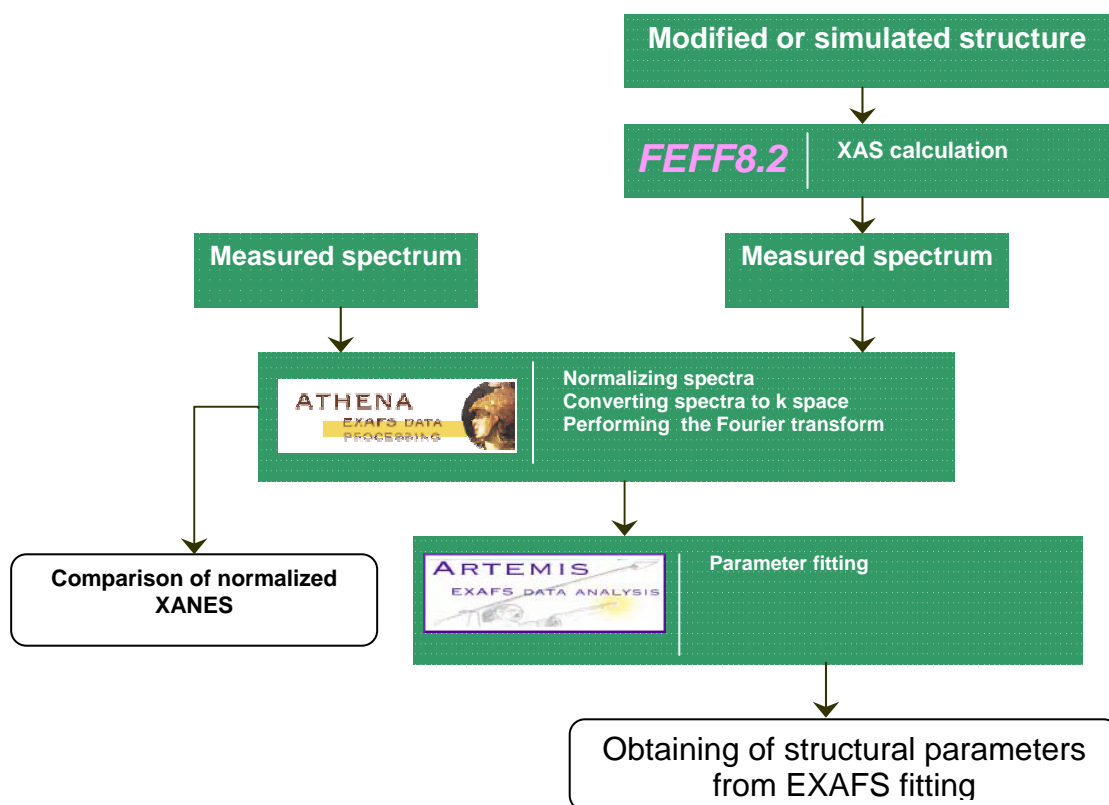


Figure 5.1 Summarized of procedure for studying of disorder system by XAS

REFERENCES

REFERENCES

- Ankudinov, A. L., Ravel, B., Rehr, J. J., and Conradsan, S. D. (1998). Real-space multiple-scattering calculation and interpretation of x-ray-absorption near-edge structure. **Phys. Rev. B** 58: 7565.
- Bakó, I., Hutter, J., and Pálinkás, G. (2002). Car–Parrinello molecular dynamics simulation of the hydrated calcium ion. **J. Chem. Phys.** 117: 9838.
- Bernal-Uruchurtu, M. I. and Ortega-Blake, I. (1995). A refined Monte Carlo study of Mg^{2+} and Ca^{2+} hydration. **J. Chem. Phys.** 103: 1588.
- Bracewell, R. N (2000). **The Fourier Transform and Its Applications**. Boston: McGraw Hill
- Brown, E. M. and MacLeod, R. J. (2001). Extracellular calcium sensing and extracellular calcium signaling. **Physiol. Rev.** 81: 239.
- Caffrey, M. (2003). Membrane protein crystallization. **J. Struct. Biol.** 142: 108.
- Dang, L. X., Schenter, G. K., Glezakou, V-A., and Fulton, J. L. (2006). Molecular simulation analysis and x-ray absorption measurement of Ca^{2+} , K^{+} and Cl^{-} ions in solution . **J. Phys. Chem. B** 110: 23644.
- Dodge Jr, F. A. and Rahamimoff, R. (1967). Co-operative action of calcium ions in transmitter release at the neuromuscular junction. **J. Physiol.** 193: 419.
- D'Angelo, P., Petit, P.-E., and Pavel, N. V. (2004). Double-electron excitation channels at the Ca^{2+} K-edge of hydrated calcium ion. **J. Phys. Chem. B** 108: 11857.

- Floris, F. M., Persico, M., Tani, A., and Tomasi, J. (1994). Hydration shell structure of the calcium ion from simulations with ab initio effective pair potentials. **Chem. Phys. Lett.** 227: 126.
- Fulton, J. L., Heald, S. M., Badyal, Y. S., and Simonson, J. M. (2003). Understanding the effects of concentration on the solvation structure of Ca^{2+} in aqueous solution. I: The perspective on local structure from EXAFS and XANES. **J. Chem. Phys. A** 107: 4688.
- Futsuhara, M., Yoshioka, K., and Takai, O. (1998). Optical properties of zinc oxynitride thin films. **The Solid Films** 317: 322.
- Hewish, N. A., Neilson, G. W., and Enderby, J. E. (1982). Environment of Ca^{2+} ions in aqueous solvent. **Nature** 297: 138.
- Izaki, M. and Omi, T. (1996). Transparent zinc oxide films prepared by electrochemical reaction. **Appl. Phys. Lett.** 68: 2439
- Jalilehvand, F., Spångberg, D., L-Reis, P., Hermansson, K., Persson I., and Sandström, M. (2001). Hydration of the calcium ion. An EXAFS, large-angle x-ray scattering, and molecular dynamics simulation study. **J. Am. Chem. Soc.** 123: 431.
- Kane, M. H., Shalini, K., Summers, C. J., Varatharajan, R., Nause, J., Vestal, C. R., Zhang, Z. J., and Ferguson, L. T. (2005). Magnetic properties of bulk $\text{Zn}_{1-x}\text{Mn}_x\text{O}$ and $\text{Zn}_{1-x}\text{Co}_x\text{O}$ single crystals. **J. Appl. Phys.** 97: 023906.
- Kuriyama, K., Takahashi, Y., and Sunohara, F. (1993). Structural, electrical and optical properties of zinc nitride thin films prepared by reactive rf magnetron sputtering. **Phys. Rev. B** 48: 2781.

- Los Alamos National Laboratory. (2001). Zinc fact [On-line]. Available: <http://chemistry.about.com/od/elementfacts/a/zinc.htm>
- Marder, M. P. (2000). **Condensed Matter Physics**. Toronto: John Wiley & Sons Limited.
- Moriga, T., Sakamoto, T., Saki, R., Murai, K., Nakabayashi, I., and Metson, J. B. (2005). Zinc oxynitride powders examined by x-ray absorption near edge spectroscopy. **Physica Scripta** T115: 312.
- Murai, A., Thompson, D. B., Mishra, U. K., Nakamura, S., and DenBaars, S. P. (2008). ZnO cone-shaped blue light emitting diodes. **Proc. SPIE** 6895: 68950N.
- Nanto, H., Minami, T., Shooji, S., and Takata, S. (1984). Electrical and optical properties of zinc oxide thin films prepared by rf magnetron sputtering of transparent electrode applications. **J. Appl. Phys.** 55: 1029.
- Periole, X., Allouche, D., Daudey, J-P., and Sanejouand, Y.H. (1997). Simple two-body cation–water interaction potentials derived from ab initio calculations. comparison to results obtained with an empirical approach. **J. Phys. Chem. B** 101: 5018.
- Ravel, B. and Newville, M. (2005). ATHENA, ARTEMIS, HEPHAESTUS: data analysis for X-ray absorption spectroscopy using IFEFFIT. **J. Synchrotron Rad.** 12: 537.
- Rehr, J. J. and Albers, R. C. (2000). Theoretical approaches to x-ray absorption fine structure. **Rev. Mod. Phys.** 72: 621.

- Schwenk, C. F. and Rode, B. M. (2004). Ab initio QM/MM MD simulations of the hydrated Ca^{2+} ion. **Pure Appl. Chem.** 76: 37.
- Shull, C. G. and Samuel Smart, J. (1949). Detection of antiferromagnetism by neutron diffraction. **Phys. Rev.** 76: 1256.
- Thienprasert, J. T., Nukeaw, J., Sungthong, A., Porntheeraphat, S., Singkarat, S., Onkaw, D., Rujirawat, S., and Limpijumnong, S. (2008). Local structure of indium oxynitride from x-ray absorption spectroscopy. **J. App. Phys. Lett.** 93: 051903.
- Tongraar, A., private communication.
- Wang, Z. L. J. (2004). Zinc oxide nanostructures: growth, properties and applications. **Phys. Condens. Matter** 16: R829.

APPENDIX

Abstract submitted for the 34th Congress on Science and Technology of Thailand

โครงสร้างไฮเดรชันรอบแคลเซียมโดยการดูดกลืนรังสีเอ็กซ์

**CALCIUM HYDRATION STRUCTURE VERIFIED BY X-RAY
ABSORPTION SPECTROSCOPY**

ธีรวัฒน์ ม่อนหน่อ,¹ จิรโรจน์ ต.เทียนประเสริฐ,¹ อนันต์ ทองระอา,² ชุกิจ ลิ้มปิจำนงค์¹ และ สาโรช
รุจิรวรรณ¹

Teerawat Monnor,¹ Jiraroj T-Thienprasert,¹ Anan Tongraar,² Sukit Limpijumnong¹
and Saroj Rujirawat¹

¹School of Physics, Suranaree University of Technology and National Synchrotron
Research Center, Nakhon Ratchasima 30000, Thailand

²School of Chemistry, Suranaree University of Technology, Nakhon Ratchasima 30000,
Thailand

บทคัดย่อ: แบบจำลองการเรียงตัวโมเลกุลของน้ำรอบไอออนแคลเซียมเป็นฟังก์ชันของเวลาได้ถูก
คำนวณโดยใช้วิธี Quantum mechanics/Molecular mechanics (QM/MM) หลังจากนั้น
แบบจำลองได้ถูกใช้ในการจำลองสเปกตรัมการดูดกลืนรังสีเอ็กซ์โดยเทคนิค First principles
calculations ในช่วงการดูดกลืน K-edge ทั้งในย่าน x-ray absorption near edge structures
(XANES) และย่าน Extended x-ray absorption fine structure (EXAFS) สเปกตรัมที่ได้จาก
การคำนวณสอดคล้องเป็นอย่างดีกับสเปกตรัมที่ได้จากการวัดการดูดกลืนรังสีเอ็กซ์ของสารละลาย
ไอออนแคลเซียม ซึ่งทำการทดลองที่ระบบลำแสงที่ 8 ของห้องปฏิบัติการแสงสยาม ศูนย์
ปฏิบัติการวิจัยเครื่องกำเนิดแสงซินโครตรอนแห่งชาติ ความสอดคล้องนี้แสดงว่าการทดลองการ
ดูดกลืนรังสีเอ็กซ์ร่วมกับการคำนวณระดับ First principles สามารถยืนยันความถูกต้องของ
แบบจำลองการเรียงตัวของโมเลกุลน้ำในชั้นรอบไอออนในน้ำได้

Abstract: Dynamic structure of water molecules around Ca^{2+} was determined by
quantum mechanics/molecular mechanics (QM/MM) modeling. Based on first
principles calculations, the dynamic structure was used to simulate the x-ray
absorption spectra [x-ray absorption near edge structures (XANE) and extended x-ray
absorption fine structure (EXAFS)]. The calculated spectrum is in good agreement
with the x-ray absorption spectroscopy (XAS) measurement from beam line 8 of the
Siam Photon Laboratory, National Synchrotron Research Center. This shows that
XAS measurement can be used to verify the hydration shells of ions in aqueous
solution when used in conjunction with first principles simulations.

Keyword: x-ray absorption spectroscopy, first principles calculation, calcium ion

CURRICULUM VITAE

Mr. Teerawat Monnor

Date of birth: 28 July 1984

Place of birth: Lamphun, Thailand

Nationality: Thai

Education

2003–2007 Chiang Mai University, Chiang Mai, Thailand

Bachelor of Science (Physics)

2007-present Currently enrolling in Master degree majoring in Physics,
School of Physics, Institute of Science, Suranaree University of
Technology, Nakhon Ratchasima, Thailand